Bulletin of the Seismological Society of America, Vol. 98, No. 1, pp. 220–240, February 2008, doi: 10.1785/0120060002

Ground-Motion Attenuation Relationships for Subduction-Zone Earthquakes in Northeastern Taiwan

by Po-Shen Lin and Chyi-Tyi Lee

Abstract Subduction zone earthquakes have not been taken into special consideration in most previous probabilistic seismic hazard analyses (PSHA) in Taiwan. However, they may be critical to properly analyze the earthquake hazard in metropolitan Taipei, so they need to be studied. Strong-motion data from subduction zone earthquakes, of both interface and intraslab types, obtained by the TSMIP and SMART1 arrays in northeastern Taiwan, are used to establish the attenuation equations for peak ground acceleration (PGA) and response spectral acceleration (SA). The resultant PGA and SA attenuation equations include two site classes and two earthquake source types. The ground-motion values predicted by these attenuation equations are higher than those obtained from the crustal earthquake attenuation equations previously used in Taiwan but are lower than those predicted by the attenuation equations for worldwide subduction zone earthquakes.

Introduction

Large earthquakes can inflict severe loss of life and property, especially when they occur in densely populated metropolitan areas. This could happen in Taipei City, which is located in northern Taiwan where the Philippine Sea plate is subducting beneath the Eurasian plate. Two large subduction zone earthquakes have occurred in this region: the 1815 Taipei earthquake, *M* 6.5 (Hsu, 1983), and the 1909 Taipei earthquake, *M* 7.3, which caused eight deaths as well as property loss (Cheng and Yeh, 1989). The 1909 Taipei earthquake occurred directly underneath the area (80-km depth). Should such a large earthquake occur now, the loss of life and property could be several hundred times greater than that of historical cases, simply because there are now many high-rise buildings situated on the soft and deep basin deposits.

To estimate the hazard level of an earthquake for a specific area, one can perform probabilistic seismic hazard analysis (PSHA). One of the most important parameters in PSHA is the ground-motion attenuation relationship, which is used to estimate the ground-motion value for an earthquake, given the magnitude, distance, and site condition. An appropriate attenuation equation cannot only help us to understand the characteristics of ground-motion attenuation, but can also predict the ground-motion values for a site so that earthquake-resistant structures can be appropriately designed.

Studies on ground-motion attenuation relationships have already been done in other countries (e.g., Kanai *et al.*, 1966; Campbell, 1981; Joyner and Boore, 1981; Crouse *et al.*, 1988; Fukushima and Tanaka, 1990; Abrahamson and Silva, 1997; Campbell, 1997) as well as in Taiwan (Tsai and Bolt, 1983; Tsai *et al.*, 1987; Chen, 1991; Ni and Chiu, 1991; Wang, 1991; Hwang, 1995; Loh, 1996; Shin, 1998; Liu, 1999; Chang *et al.*, 2001; Wu *et al.*, 2001; Liu and Tsai, 2005). However, big differences exist in the results obtained from attenuation equations, arising from the different data sets utilized (Abrahamson and Shedlock, 1997).

Recently, some researchers have pointed out that the ground-motion attenuation conditions for subduction zone earthquakes and shallow crustal earthquakes are different (Crouse *et al.*, 1988; Crouse, 1991; Molas and Yamazaki, 1995; Youngs *et al.*, 1997). Many of the existing attenuation equations used in Taiwan are based mainly on either data for shallow crustal earthquake or mixed usage, without consideration being given to the apparent differences between shallow crustal and subduction zone earthquakes.

Here we try to understand the ground-motion attenuation characteristics of subduction zone earthquakes that occur in northeastern Taiwan and to establish a set of appropriate attenuation equations for subduction zone earthquakes for PSHA studies, making reference to the Crouse (1991) and Youngs *et al.* (1997) attenuation models and using data from subduction zone earthquakes in northeast Taiwan for the analyses. In addition to the determination of the peak ground acceleration (PGA) attenuation equation, we also determine the spectral acceleration (SA) attenuation equations for engineering application purposes.

Seismotectonics of Northeastern Taiwan

Taiwan is located at the convergent boundary between the Philippine Sea plate and the Eurasian plate. The Philippine Sea plate is moving towards the northwest at a rate of

about 7 cm/yr (Seno, 1977; Seno *et al.*, 1993) or 8 cm/yr (Yu *et al.*, 1997), while the Luzon arc at the leading edge of the Philippine Sea plate collides with the Eurasian plate in eastern Taiwan. In northeastern Taiwan, the Philippine Sea plate is subducting beneath the Eurasian plate. The strike of the Ryukyu trench is oriented approximately northwest–southeast near 121.5° E and then rotates to a more east–west strike direction toward the west of 125° E (see Fig. 1).

Based on tomography analysis, Rau and Wu (1995) showed that there is a tilted relatively high velocity layer in northern Taiwan, the location of which closely coincides with the Wadati–Benioff zone. Chen (1995) pointed out that the subduction zone in northeastern Taiwan begins subducting northward at 24° N, with a dip angle of 20°–30° at shallow depths, which changes to 50°–60° at greater depths of about 180 km.

Shen (1996) suggested that there is a subducting boundary (trench) oriented in an east–west direction, approximately located between 23.4° to 23.7° N. It dips to the north at a low inclination angle. The relative motion between the plates along this boundary should occur in nonearthquake form within a depth of 20 km, with weak coupling at the plate boundary. On the Philippine Sea plate, at a depth between 80 to 150 km, the velocity of the northward subduction becomes slower; the inserted depth of the plate could be as much as 300 km, so considerable resistance should appear at this depth (Shen, 1996).

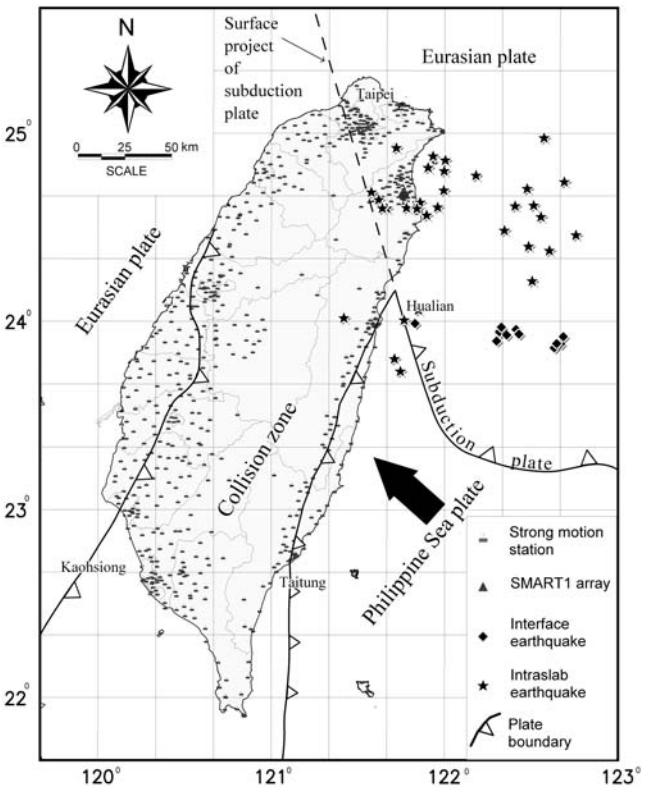

Figure 1. Locations of earthquakes and strong-motion stations used in this study. A star indicates the epicenter of an intraslab earthquake. A rhomboid indicates the epicenter of an interface earthquake. A rectangle with a flag shows the location of a strong-motion station.

Kao *et al.* (1998) utilized background earthquake data from 62 earthquakes with body-wave magnitudes (m_b) of 5.5–6.6 to describe the seismotectonic regions in northeastern Taiwan, which are (1) the collision seismic zone, (2) the interface seismic zone (ISZ), (3) the Wadati Benioff seismic zone (WBSZ), (4) the lateral compression seismic zone, and (5) the Okinawa seismic zone. Our interests are the ISZ and the WBSZ.

Data Acquisition and Analysis

The Central Weather Bureau (CWB) routinely reports earthquake magnitudes in local magnitude (M_L), making this the type most frequently used in previous studies in Taiwan. However, when it comes to large magnitude earthquakes ($M_L > 6.5$), there is a saturation problem that arises with the Richter magnitude scale (Heaton *et al.*, 1986). To counteract this problem, the moment magnitude scale, M_w (Hanks and Kanamori, 1979), which is directly related to fault rupture area and earthquake energy, is used as the magnitude parameter in the present attenuation model study. There are two sources for obtaining the moment magnitudes: the moment magnitude (M_w-HVD) released by the Harvard Centroid Moment Tensor database (Harvard CMT) and the moment magnitude (M_w-BATS) released by the Broadband Array in Taiwan for Seismology (BATS). However, given that systematic error is likely to occur in one of these data sets (Huang *et al.*, 2000), we convert the BATS moment magnitude values, using the conversion equation proposed by Huang *et al.* (2000), to M_w-HVD, thus keeping the magnitudes on the same scale.

In some other studies, the local magnitude M_L was converted to the moment magnitude M_w (Tsai and Wen, 1999; Wu *et al.*, 2001). However, in these studies the difference in the conversion relationship between deep-focus earthquakes (depth >50 km) and shallow-focus earthquakes was not considered. In the present study, we formulate a conversion equation (equation 1) suitable for converting M_L to M_w for shallow-focus and deep-focus earthquakes, respectively, as shown in Figure 2, which utilizes the M_L and M_w data from the earthquake catalogs. Our conversion equation passes through the origin and becomes saturated when M_L is large. The thick solid line indicates the M_L to M_w conversion proposed in this study, the long dashed line represents the conversion proposed by Liu *et al.* (1999), and the short dashed line represents the conversion by Wu *et al.* (2001). We calculate the R^2 (R-square) value to see if our relation is better than the other two relations for these two groups of data. For shallow earthquake data, R^2 for our relation, Wu *et al.* (2001) and Tsai and Wen (1999) are 0.842, 0.826, and 0.818, respectively; for deep earthquake data, R^2 for our relation, Wu *et al.* (2001) and Tsai and Wen (1999) are 0.712, 0.427, and 0.350, respectively. Higher R^2 values represent

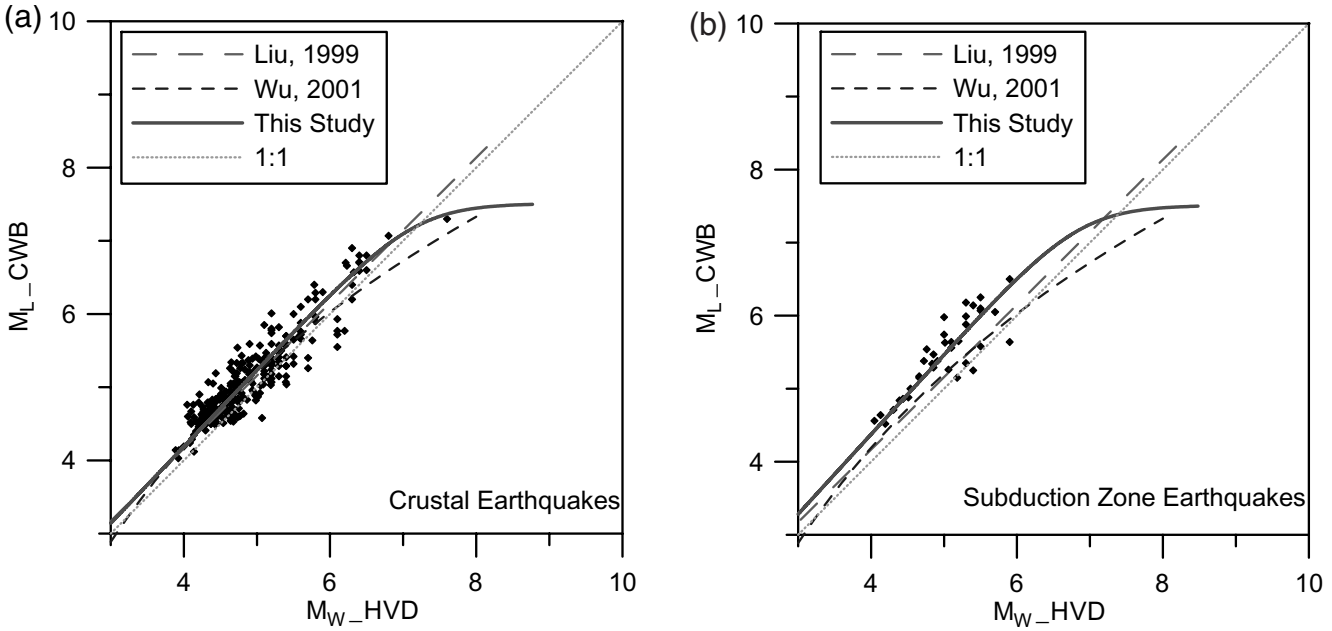

Figure 2. Comparison of the relation between the magnitude scales M_L and M_w by different studies for (a) crustal earthquakes and (b) subduction zone earthquakes.

better goodness of fit of a model. Our M_L to M_w conversion equation has the highest R^2 value and was used in this study:

$$M_w = 7.2 - \log\left[10^{7.2} \times \frac{e^{-\beta \times M_L} - e^{-\beta \times mu}}{1 - e^{-\beta \times mu}}\right],$$

$$\beta = b \times \ln(10)$$

for shallow earthquakes $b = 0.955$ and $mu = 7.51$,

for deep earthquakes $b = 0.9144$ and $mu = 7.51$. (1)

Youngs *et al.* (1997) divided the subduction zone earthquakes into two types: interface and intraslab. Subduction zone interface earthquakes are shallow angle thrust events that occur at the interface between the subducting and overriding plates. Subduction zone intraslab earthquakes occur within the subducting oceanic plate and are typically high-angle normal-faulting events responding to down-dip tension in the subducting plate. Tichelaar and Ruff (1993) suggested that interface earthquakes mostly occur at depths of less than 50 km so that earthquakes that occur at depths greater than 50 km are regarded as intraslab earthquakes. In this study, the data for earthquakes in the study area are collected from the earthquake catalog and classified according to this criterion. We use the strong-motion data from the Taiwan strong-motion instrumentation program (TSMIP) (Liu *et al.*, 1999) as well as some of the strong-motion records from the SMART1 array, a cooperative program between the Institute of Earth Sciences, Academia Sinica, and the University of California at Berkeley. The relevant earthquake parameters used in this analysis are listed in Table 1. The distribution of the epicenters of subduction zone earthquakes as well as the locations of strong-motion stations are presented in Figure 1. We lacked ground-motion data for large magnitude subduction zone earthquakes in Taiwan. For this reason, foreign ground-motion data for large magnitude subduction zone earthquakes have been added. The relevant earthquake parameters of these earthquakes are shown in Table 2. The result is a total of 54 earthquakes, 17 of which were interface earthquakes, and 37 intraslab earthquakes. This data set includes 4823 sets of three-component digital strong-motion data. Distributions of the magnitude and hypocentral distances in this data set are shown in Figure 3. The magnitudes of the intraslab earthquakes are between M_w 4.1 and 6.7, with distances of 40– 600 km. The magnitudes of the interface earthquakes are from M_w 5.3 to 8.1, with distances of 20–300 km.

The earthquake records were screened prior to processing. Pristine earthquake records were subjected to baseline correction and then were plotted as time histories. The earthquake records were handpicked; only good quality records were picked, and damaged or questionable records were excluded. Records with square waves, due to PGA values that were too small, were also discarded. After screening, there were 4383 sets of data available.

In regression analysis, the geometric mean of the two horizontal PGAs is used as the ground-motion PGA. We adopted the moment magnitudes released by the Harvard Seismology Center for the earthquake magnitude parameter. If the Harvard data were not available, a magnitude parameter value was obtained by converting the local magnitude to the moment magnitude. Hypocentral distance was used for

Table 1

Parameters of the Earthquakes in Northeast Taiwan Used in This Study

Number	Date (mm/dd/yyyy)	Time	Longitude	Latitude	Depth	M_L	M_w	Record Number
			Interface Earthquakes					
1	09/21/1983	19:20:40	122.317	23.9381	18	6.5	6.4	8
2	11/14/1986	21:20:04	121.833	23.9918	15	6.5	7.3	15
3	09/28/1992	14:06:03	122.673	23.8828	17.58	5.72	6.1	12
4	03/17/1994	11:28:01	122.416	23.9598	20.2	5.65	5.5	21
5	05/23/1994	05:36:02	122.688	23.9215	7.21	5.77	6.1	33
6	05/23/1994	15:16:59	122.636	23.8627	5.54	6	5.9	117
7	04/03/1995	11:54:40	122.432	23.9355	14.55	5.88	5.6	140
8	04/03/1995	22:33:24	122.320	23.9472	3.94	5.35	5.3	1
9	03/05/1996	14:52:27	122.362	23.9302	6	6.4	6.3	234
10	03/05/1996	17:32:09	122.303	23.8985	10.81	5.96	5.8	146
11	03/29/1996	03:28:54	122.331	23.9718	5.79	5.64	5.7	49
12	08/10/1996	06:23:06	122.650	23.8850	5.65	5.76	5.6	43
			Intraslab Earthquakes					
1	01/20/1994	05:50:15	121.852	24.065	49.5	5.58	5.50	213
2	02/01/1994	22:44:27	122.693	24.747	115.6	6.13	5.62*	75
3	10/12/1994	09:08:22	122.000	24.805	73.1	5.67	5.19*	90
4	03/24/1995	04:13:51	121.861	24.638	76	5.64	5.10	185
5	04/24/1995	10:04:00	121.622	24.652	63.1	5.28	4.83*	132
6	06/25/1995	06:59:07	121.669	24.606	39.9	6.5	5.90	350
7	8/20/1995	09:25:03	121.580	24.692	56.9	4.92	4.50*	97
8	12/01/1995	03:17:04	121.643	24.606	45.1	5.72	5.24*	189
9	01/22/1996	19:22:57	121.724	24.928	66.9	5.11	4.67*	121
10	07/29/1996	20:20:53	122.347	24.489	65.7	6.14	5.40	305
11	12/15/1996	18:56:26	121.422	24.022	71.4	4.81	4.40*	23
12	04/13/1997	17:45:13	121.714	23.805	45.5	5.56	5.10	187
13	04/27/1997	23:59:32	121.962	24.612	60.6	5.15	4.43	45
14	07/15/1997	11:05:33	122.516	24.622	86.6	6.1	5.50	177
15	09/28/1997	07:54:26	121.783	24.609	68.6	5.01	4.58*	49
16	10/11/1997	18:24:25	122.576	24.981	146.4	6.07	5.50	53
17	05/02/1998	05:37:42	122.558	24.561	86.1	5.63	4.81	44
18	05/09/1998	20:53:39	121.907	24.823	83.6	5.38	4.70	135
19	04/04/1999	04:59:03	121.936	24.8835	88.95	5.82	5.01	166
20	04/30/1999	05:44:40	121.899	24.5698	66.75	4.8	4.39*	34
21	06/03/1999	16:11:43	122.487	24.4037	61.67	6.18	5.24	238
22	07/11/1999	20:25:11	121.843	24.605	73.17	5.07	4.64*	124
23	09/30/1999	09:49:45	121.998	24.7015	70.55	5.53	5.06*	121
24	12/06/1999	18:14:34	122.006	24.862	100.16	4.78	4.37*	10
25	04/14/2000	01:36:39	122.508	24.2195	48.31	5.19	4.31	19
26	06/28/2000	11:35:02	122.409	24.6182	90.79	5.34	4.89*	34
27	07/10/2000	08:32:58	121.748	23.7385	43.71	4.83	4.42*	57
28	07/24/2000	22:10:36	122.479	24.7112	110.05	5.74	5.00	109
29	02/16/2001	23:13:09	122.76	24.4642	60.55	5.98	5.00	90
30	04/24/2001	08:26:38	122.183	24.7815	82.77	4.78	4.37*	13
31	06/13/2001	13:17:54	122.607	24.3812	64.41	6.25	5.50	293
32	07/09/2001	15:20:48	121.769	24.011	43.39	5.13	4.39	87

*M_w was estimated from the M_L–M_w relation for these values.

the distance parameter. Site classification of TSMIP strong-motion stations proposed by Lee *et al.* (2001) was used, and sites were simplified as rock sites (B and C types) or soil sites (D and E types).

Attenuation Model and Regression Method

Seismic waves propagate from the hypocenter to the site through an irregular layered medium, in a highly complicated manner. A strong-motion record is thus intimately related to the characteristics of the source, transmission path, and site effects. A ground-motion attenuation model should include the earthquake source parameter, propagation parameter, site parameter, and ground-motion parameter. There are two methods for deciding the ground-motion attenuation model: one uses empirical equations acquired through the regression of ground-motion data, and the other synthesizes the theoretical ground-motion of the earthquake through modeling. It is also possible to use both methods jointly, first by obtaining theoretically the suggested functional form, followed by fitting the empirical equations with observational data.

Table 2
Parameters of the Earthquakes in Foreign Areas Added in This Study

Number	Date (mm/dd/yyyy)	Time	Longitude	Latitude	Depth	M_L	M_w	Record Number
			Interface Earthquakes					
1	02/28/1979	21:27	−141.593	60.642	15		7.1	2
2	09/19/1985	13:17	−102.530	18.190	27		8.1	16
3	09/21/1985	01:37	−101.650	17.800	30		7.6	11
4	04/25/1989	14:29	−99.330	16.770	19		7.1	15
5	04/25/1992	18:06	−124.316	40.368	15		7	10
			Intraslab Earthquakes					
1	04/29/1965	07:28	−122.300	47.40	59		6.7	2
2	05/23/1994	01:41	−100.530	18.17	55		6.3	16
3	05/22/1997	07:50	−101.600	18.68	70		6.6	12
4	10/25/1999	20:31	175.920	−38.57	161	6.9	6	54
5	07/28/2001	07:32	−155.116	59.03	131		6.6	1

Attenuation equations are commonly comprised of three parts related to the source, geometric spreading, and inelastic attenuation. When a site effect is considered, then the general form (Joyner and Boore, 1981) becomes

$$y = B_1 f_1(M) f_2(R) f_3(M, R) f_4(P_i) \varepsilon, \tag{2}$$

in which y is the ground-motion parameter, B_1 is a constant, $f_1(M)$ is a function relevant to the magnitude, $f_2(R)$ is a function related to distance, $f_3(M, R)$ is a function related to magnitude and distance, $f_4(P_i)$ is a parameter related to site effects or the effect of structure, and ε represents the random error.

$f_1(M)$ is generally taken as an exponential function of magnitude, that is,

$$f_1(M) = e^{b_2 M}. \tag{3}$$

The origin of this form is related to the fundamental definition of magnitude, which is the intensity of the ground-motion measured in logarithmic form (Richter, 1958). The form of the function $f_2(R)$ is

$$f_2(R) = e^{b_4 R}[R + b_5]^{-b3}, \tag{4}$$

where $[R + b_5]^{-b3}$ is the attenuation induced by geometric spreading, b_3 represents the geometric attenuation rate, $e^{b_4 R}$ is used to calculate the inelastic attenuation, b_4 represents the inelastic attenuation coefficient, and b_5 functions as a limit for the ground-motion parameter when the distance approaches zero, so that saturation can be reasonably attained. Furthermore, $f_2(R)$ may also be expressed as

$$f_2(R) = e^{b_4 R}(\sqrt{R^2 + b^2})^{-b_3}, \tag{5}$$

where $\sqrt{R^2 + b^2}$ is comparable to the definition for the hypocentral distance and also prevents the value of y from becoming infinite.

The function $f_3(M, R)$ mainly expresses the attenuation uncertainty as ground motion increases with distance R, for earthquakes with different magnitudes. In general, $f_3(M, R) = 1$; however, Campbell (1981) defined

$$f_3(M, R) = [R + b_5 M^{b_6}]^{-b_3} \tag{6}$$

and $f_2(R)$ as

$$f_2(R) = e^{b_4}. \tag{7}$$

In Campbell's attenuation model (Campbell, 1981), the attenuation coefficient b_6 is generally positive, indicating that the attenuation of larger earthquakes would be relatively faster than the attenuation of smaller slower earthquakes: this characteristic is known as magnitude saturation.

Without considering factors such as the site effect, fault rupture type, and structural effect, it is possible to express equation (2) in logarithmic form as follows:

$$\ln y = b_1 + \ln[f_1(M)] + \ln[f_2(R)] + \ln[f_3(M, R)] + \ln \varepsilon, \tag{8}$$

in which $b_1 = \ln B_1$. Assuming that ε has a lognormal distribution, then $\ln \varepsilon$ has a normal distribution, also known as a Gaussian distribution.

Youngs *et al.* (1995) found that regression random error is related to the earthquake magnitude and that, as the magnitude increases, the standard deviation decreases. Tsai (1998) used a specific barrier model to simulate seismic waves and obtain the near field PGA. He discovered that the greater the cutoff frequency ($f_{\max}$) set for a seismic source, the higher the PGA value. Furthermore, the smaller the magnitude, the greater the PGA's exponential standard deviation, $\sigma_{\ln \mathrm{PGA}}$. In the near field, the nearer the fault distance, the greater the $\sigma_{\ln \mathrm{PGA}}$. The findings of Youngs *et al.* (1995) and Tsai (1998) not only affect the results of the PSHA but can also improve the overconservative situation, due to overestimation of the standard deviation of large

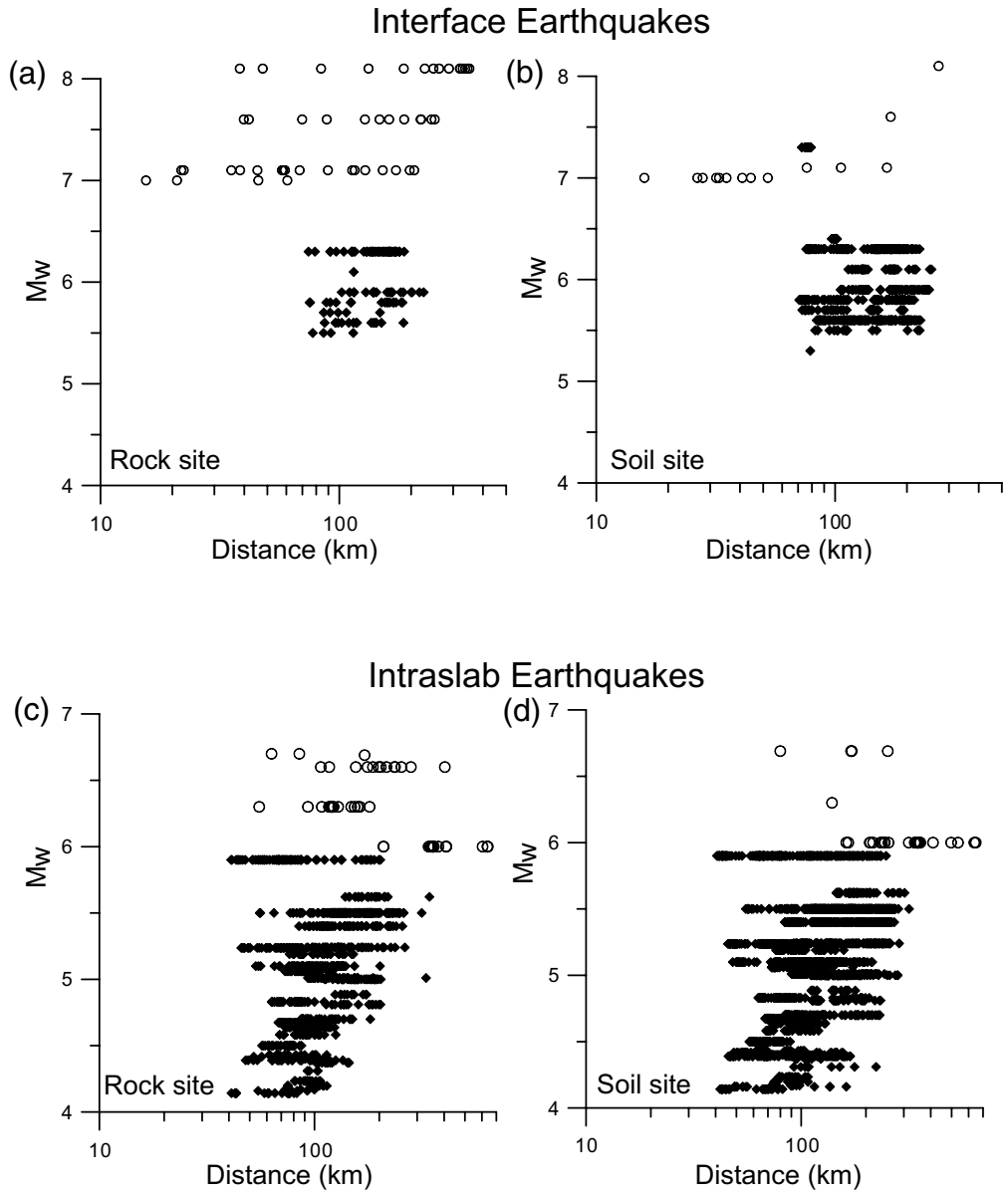

Figure 3. The magnitude and distance distribution of the strong-motion data set used in this study. The solid rhomboids represent data from the Taiwan area; the open circles represent data from other areas.

magnitude earthquakes. Recently Abrahamson and Silva (1997), Campbell (1997), Youngs *et al.* (1997), Toro *et al.* (1997), and Sadigh *et al.* (1997) considered the regression error term in their respective attenuation equations as a linear function of magnitude $\varepsilon(M)$.

For the purpose of establishing a uniform hazard response spectrum for the PSHA, y in a broader sense refers to the amplitude of the response spectrum for the structure period T. Equation (2) may now be rewritten as

$$y(T) = f_1(M,T)f_2(R,T)f_3(M,R,T)f_4(Pi,T)\varepsilon(T). \quad (9)$$

For a given earthquake force, a single degree of freedom system will have different responses with different natural periods and damping ratios. The response spectrum is the maximum response of a single degree of freedom oscillator with a given damping value for a given period. To calculate the response spectrum, we make use of the entire acceleration time history. To find an earthquake's response spectrum, we calculate the 5% critical-damping ratio response spectrum, with periods ranging from 0.01 to 5 sec, at sampling intervals of 0.01 sec. During the actual regression analysis of the response spectrum attenuation, several periods were computed from each record (0.01, 0.02, 0.03, 0.04, 0.05, 0.06, 0.09, 0.1, 0.12, 0.15, 0.17, 0.2, 0.24, 0.3, 0.36, 0.4, 0.46, 0.5, 0.6, 0.75, 0.85, 1.0, 1.5, 2.0, 3.0, 4.0, 5.0); regression analysis was then conducted in order.

In regression analysis, the regression model should be selected first. In this study, we selected only one single model, meaning that in terms of data parameter distribution, the study was not self-contained in relation to analysis. With due consideration of the physical properties of the attenuation model and its adequacy for use, we also refer to the published subduction zone earthquake ground-motion attenuation models (Crouse, 1991; Youngs *et al.*, 1997), to establish the present attenuation model. The PGA attenuation form is

$$\ln(\mathrm{PGA}_{ij}) = C_1 + C_2 M_i + C_3 \ln(R_{ij} + C_4 e^{C_5 M_i}) + C_6 H_i + C_7 Z_t + \ln \varepsilon, \quad (10)$$

where i denotes the ith earthquake, j denotes the jth station that made the ith earthquake record, PGA(g) is the geometric mean of the two horizontal PGA values, M is the moment magnitude M_w in this equation, R is the hypocentral distance (km), H is the focal depth (km), Z_t represents the earthquake type ($Z_t = 0$, interface; $Z_t = 1$, intraslab), and $\ln \varepsilon$ is a random error. The response spectrum attenuation form for the other periods is

$$\ln(\mathrm{SA}_{ij}) = C_1 + C_2 M_i + C_3 \ln(R_{ij} + \alpha_1 e^{\alpha_2 M_i}) + \alpha_3 H_i + \alpha_4 Z_t + \ln \varepsilon. \quad (11)$$

Here, SA is the amplitude of the response spectrum for each period; the definitions for M, R, H, and Z_t are similar to the PGA attenuation form.

The least-squares basis for nonlinear regression model is

$$S = \sum_{i=1}^{n} \sum_{j=1}^{m} [\ln Y_{ij} - f(M_i, R_{ij}, H_i, Z_{ti}, C)]^2, \quad (12)$$

in which $f(M_i, R_{ij}, H_u, Z_{ti}, C)$ are the mean responses for the ith earthquake and jth station following the nonlinear function $f(M_i, R_{ij}, H_u, Z_{ti}, C)$. The basis of a least-squares S should be minimized through nonlinear regression; parameters $C_1, C_2, \ldots, C_n$ are estimated for the least-squares estimation. There are two methods for obtaining the least-squares estimation—a numerical search and the standard equation. Because our problem is different from a linear regression where there commonly exists an analytical solution for the standard equation, an iterated numerical search process had to be employed. The numerical search method selected for this study was the hill-climbing search method (Russell and Norvig, 2003). In the hill-climbing search, the point for each search is only aimed at and moves toward the point closest to the target point; it never drifts far away from the target. To avoid falling into the local minimum pitfall, we improved the hill-climbing search method, renaming it the block hill-climbing search method. The first step of the block hill-climbing search method is to set an initial search block and then to give it an initial value. One searches for this relatively small value for this block. In the second step one uses the relatively small value to redefine the search block, after which the relatively small value is again selected. These steps are repeated until the search block approaches the minimum value. Stopping the search at the defining search block involves the same two steps. We finish the search and get the minimum value.

As verified by repeated testing of the initial search block and search interval, the regression results obtained using the block hill-climbing search method were stable and reasonable.

Results and Evaluations

If the least-squares method is used to perform the regression, the data need to be weighted. Here we weighted the data given the amount of data that came from different sources. The site classification used in this study was simplified from Lee *et al.* (2001) to two groups, namely, rock sites (B and C types) and soil sites (D and E types).

Two different data sets were used in the regression analysis: one data set containing large magnitude earthquake data from foreign sources and the other one using earthquake data for the Taiwan area. The results from the latter data set were not reliable for larger magnitudes because the distribution of the data was too limited. For example, coefficient C_3, which is related to geometric spreading, was larger in this data set so that the trend of the attenuation equation showed a rather small slope ($C_3 \fallingdotseq 1.0$–1.3). Therefore, we focused on the former data set, which included large magnitude subduction zone earthquakes that occurred in foreign countries. The resultant PGA attenuation equation for rock sites is

$$\ln(\mathrm{PGA}) = -2.5 + 1.205M - 1.905 \ln(R + 0.516e^{0.6325M}) + 0.0075H + 0.275Z_t \quad (13)$$

and for soil sites is

$$\ln(\mathrm{PGA}) = -0.9 + 1.00M - 1.90 \ln(R + 0.9918e^{0.5263M}) + 0.004H + 0.31Z_t, \quad (14)$$

where PGA is the geometric mean value (acceleration of gravity) of the horizontal PGA, M is the moment magnitude, R is the hypocentral distance, H is the focal depth (kilometers), and Z_t indicates the subduction zone earthquake type; $Z_t = 0$ for interface earthquakes, and $Z_t = 1$ for intraslab earthquakes. The distribution of data used in the regression analysis was as follows: it covered 5.3–8.1 for moment magnitude, 15–630 km for hypocentral distance, and 4–161 km for focal depth. The coefficients for all other values of each period from the SA attenuation equation are tabulated in Tables 3 and 4.

A comparison of attenuation calculations for rock and soil sites, for various types of subduction zone earthquakes and various magnitudes, reveals that the estimated horizontal PGA for a soil site is always higher than that for a rock site.

This indicates that the site classification used in this study does indeed reflect the soil site amplification effects (Figs. 4 and 5).

The coefficient of the H term is positive, indicating that the horizontal PGA value increases with depth, as shown in Figure 6. The H coefficient is different for the rock sites and for soil sites, and hence, there exists a slight difference in their trend to increase with depth.

Regarding the differences between intraslab earthquakes and interface earthquakes, the Z_t coefficients are also positive, indicating that the horizontal PGA value is greater for intraslab earthquakes than for interface earthquakes, given the same magnitude and depth (Figs. 4 and 5).

Figures 7 and 8 present the horizontal PGA and SA attenuation curves for an M_w 6.0 earthquake, at rock and soil sites. A comparison at the variation in the regression coefficients with periods between rock and soil sites shows that for C_1 and C_2 coefficient trends are similar, but the C_3 coefficients have a larger difference (Fig. 9). The C_1 coefficient increased slightly as the period increased from 0.01 to 0.1 sec. When the period was greater than 0.1 sec, the C_1 coefficient decreased as the period increased, implying that the acceleration response spectrum values would gradually decrease with an increase in period when the period is greater than 0.1 sec. The C_1 coefficient showed a large change, from 0.05 to −13, for different periods. The C_2 coefficient is related to the magnitude; it slightly decreased as the period increased from 0.01 to 0.1 sec, and then it increased with the period until it reached a maximum value at 3 sec. Coefficient C_2 ranged from 0.9 to 1.9. The C_3 coefficient is related to geometric spreading; it increased continuously for a rock site. It increased slightly as the period increased from 0.01 to 0.1 sec, and then it increased with the period up to 5 sec. Coefficient C_3 ranged from −1.9 to −0.9.

The PGA attenuation equation regression error $\sigma_{\ln \varepsilon}$ is defined as

$$\sigma_{\ln \varepsilon} = \sqrt{\frac{\sum_{i=1}^{n} \{[\ln(\text{predicted})_i] - [\ln(\text{observed})_i]\}^2}{n-7}}. \quad (15)$$

The SA attenuation equation regression error $\sigma_{\ln \varepsilon}$ for each period is defined as

$$\sigma_{\ln \varepsilon} = \sqrt{\frac{\sum_{i=1}^{n} \{[\ln(\text{predicted})_i] - [\ln(\text{observed})_i]\}^2}{n-3}}. \quad (16)$$

The value of the regression error $\sigma_{\ln \varepsilon}$ will affect the PSHA results. The error may originate from a deficiency in the knowledge about earthquake characteristics and simplification of the form of the attenuation equation. This is jointly known as the modeling error in the attenuation equation (Hong and Hsu, 1993). In equation (10), the random

Table 3

Regression Coefficients of Attenuations for Rock Sites

Period	C_1	C_2	C_3	C_4	C_5	C_6	C_7	$\sigma_{\ln y}$
PGA	−2.500	1.205	−1.905	0.51552	0.63255	0.0075	0.275	0.5268
0.01	−2.500	1.205	−1.895	0.51552	0.63255	0.0075	0.275	0.5218
0.02	−2.490	1.200	−1.880	0.51552	0.63255	0.0075	0.275	0.5189
0.03	−2.280	1.155	−1.875	0.51552	0.63255	0.0075	0.275	0.5235
0.04	−2.000	1.100	−1.860	0.51552	0.63255	0.0075	0.275	0.5352
0.05	−1.900	1.090	−1.855	0.51552	0.63255	0.0075	0.275	0.537
0.06	−1.725	1.065	−1.840	0.51552	0.63255	0.0075	0.275	0.5544
0.09	−1.265	1.020	−1.815	0.51552	0.63255	0.0075	0.275	0.5818
0.10	−1.220	1.000	−1.795	0.51552	0.63255	0.0075	0.275	0.5806
0.12	−1.470	1.040	−1.770	0.51552	0.63255	0.0075	0.275	0.5748
0.15	−1.675	1.045	−1.730	0.51552	0.63255	0.0075	0.275	0.5817
0.17	−1.846	1.065	−1.710	0.51552	0.63255	0.0075	0.275	0.5906
0.20	−2.170	1.085	−1.675	0.51552	0.63255	0.0075	0.275	0.6059
0.24	−2.585	1.105	−1.630	0.51552	0.63255	0.0075	0.275	0.6315
0.30	−3.615	1.215	−1.570	0.51552	0.63255	0.0075	0.275	0.6656
0.36	−4.160	1.255	−1.535	0.51552	0.63255	0.0075	0.275	0.701
0.40	−4.595	1.285	−1.500	0.51552	0.63255	0.0075	0.275	0.7105
0.46	−5.020	1.325	−1.495	0.51552	0.63255	0.0075	0.275	0.7148
0.50	−5.470	1.365	−1.465	0.51552	0.63255	0.0075	0.275	0.7145
0.60	−6.095	1.420	−1.455	0.51552	0.63255	0.0075	0.275	0.7177
0.75	−6.675	1.465	−1.450	0.51552	0.63255	0.0075	0.275	0.7689
0.85	−7.320	1.545	−1.450	0.51552	0.63255	0.0075	0.275	0.7787
1.0	−8.000	1.620	−1.450	0.51552	0.63255	0.0075	0.275	0.7983
1.5	−9.240	1.705	−1.440	0.51552	0.63255	0.0075	0.275	0.8411
2.0	−10.200	1.770	−1.430	0.51552	0.63255	0.0075	0.275	0.8766
3.0	−11.470	1.830	−1.370	0.51552	0.63255	0.0075	0.275	0.859
4.0	−12.550	1.845	−1.260	0.51552	0.63255	0.0075	0.275	0.8055
5.0	−13.390	1.805	−1.135	0.51552	0.63255	0.0075	0.275	0.7654

The regression equation is $\ln(y) = C_1 + C_2 M + C_3 \ln(R + C_4 e^{C_5 M}) + C_6 H + C_7 Z_t$.

Table 4

Regression Coefficients of Attenuations for Soil Sites

Period	C_1	C_2	C_3	C_4	C_5	C_6	C_7	$\sigma_{\ln y}$
PGA	−0.900	1.000	−1.900	0.99178	0.52632	0.004	0.31	0.6277
0.01	−2.200	1.085	−1.750	0.99178	0.52632	0.004	0.31	0.5800
0.02	−2.290	1.085	−1.730	0.99178	0.52632	0.004	0.31	0.5730
0.03	−2.340	1.095	−1.720	0.99178	0.52632	0.004	0.31	0.5774
0.04	−2.215	1.090	−1.730	0.99178	0.52632	0.004	0.31	0.5808
0.05	−1.895	1.055	−1.755	0.99178	0.52632	0.004	0.31	0.5937
0.06	−1.110	1.010	−1.835	0.99178	0.52632	0.004	0.31	0.6123
0.09	−0.210	0.945	−1.890	0.99178	0.52632	0.004	0.31	0.6481
0.10	−0.055	0.920	−1.880	0.99178	0.52632	0.004	0.31	0.6535
0.12	0.055	0.935	−1.895	0.99178	0.52632	0.004	0.31	0.6585
0.15	−0.040	0.955	−1.880	0.99178	0.52632	0.004	0.31	0.6595
0.17	−0.340	1.020	−1.885	0.99178	0.52632	0.004	0.31	0.6680
0.20	−0.800	1.045	−1.820	0.99178	0.52632	0.004	0.31	0.6565
0.24	−1.575	1.120	−1.755	0.99178	0.52632	0.004	0.31	0.6465
0.30	−3.010	1.315	−1.695	0.99178	0.52632	0.004	0.31	0.6661
0.36	−3.680	1.380	−1.660	0.99178	0.52632	0.004	0.31	0.6876
0.40	−4.250	1.415	−1.600	0.99178	0.52632	0.004	0.31	0.7002
0.46	−4.720	1.430	−1.545	0.99178	0.52632	0.004	0.31	0.7092
0.50	−5.220	1.455	−1.490	0.99178	0.52632	0.004	0.31	0.7122
0.60	−5.700	1.470	−1.445	0.99178	0.52632	0.004	0.31	0.7280
0.75	−6.450	1.500	−1.380	0.99178	0.52632	0.004	0.31	0.7752
0.85	−7.250	1.565	−1.325	0.99178	0.52632	0.004	0.31	0.7931
1.0	−8.150	1.605	−1.235	0.99178	0.52632	0.004	0.31	0.8158
1.5	−10.300	1.800	−1.165	0.99178	0.52632	0.004	0.31	0.8356
2.0	−11.620	1.860	−1.070	0.99178	0.52632	0.004	0.31	0.8474
3.0	−12.630	1.890	−1.060	0.99178	0.52632	0.004	0.31	0.8367
4.0	−13.420	1.870	−0.990	0.99178	0.52632	0.004	0.31	0.7937
5.0	−13.750	1.835	−0.975	0.99178	0.52632	0.004	0.31	0.7468

The regression equation is $\ln(y) = C_1 + C_2M + C_3 \ln(R + C_4 e^{C_5 M}) + C_6H + C_7Z_t$.

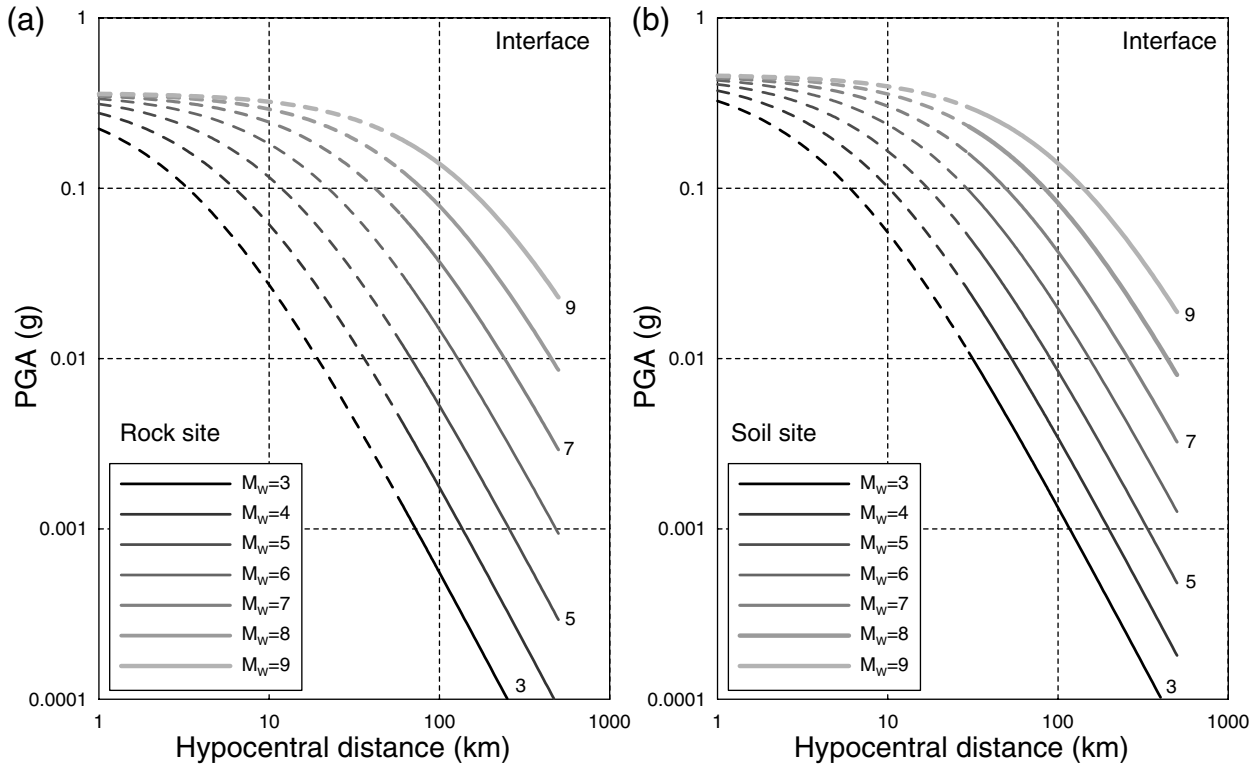

Figure 4. Results of the PGA attenuation curves for interface earthquakes at different magnitudes: (a) rock sites and (b) soil sites.

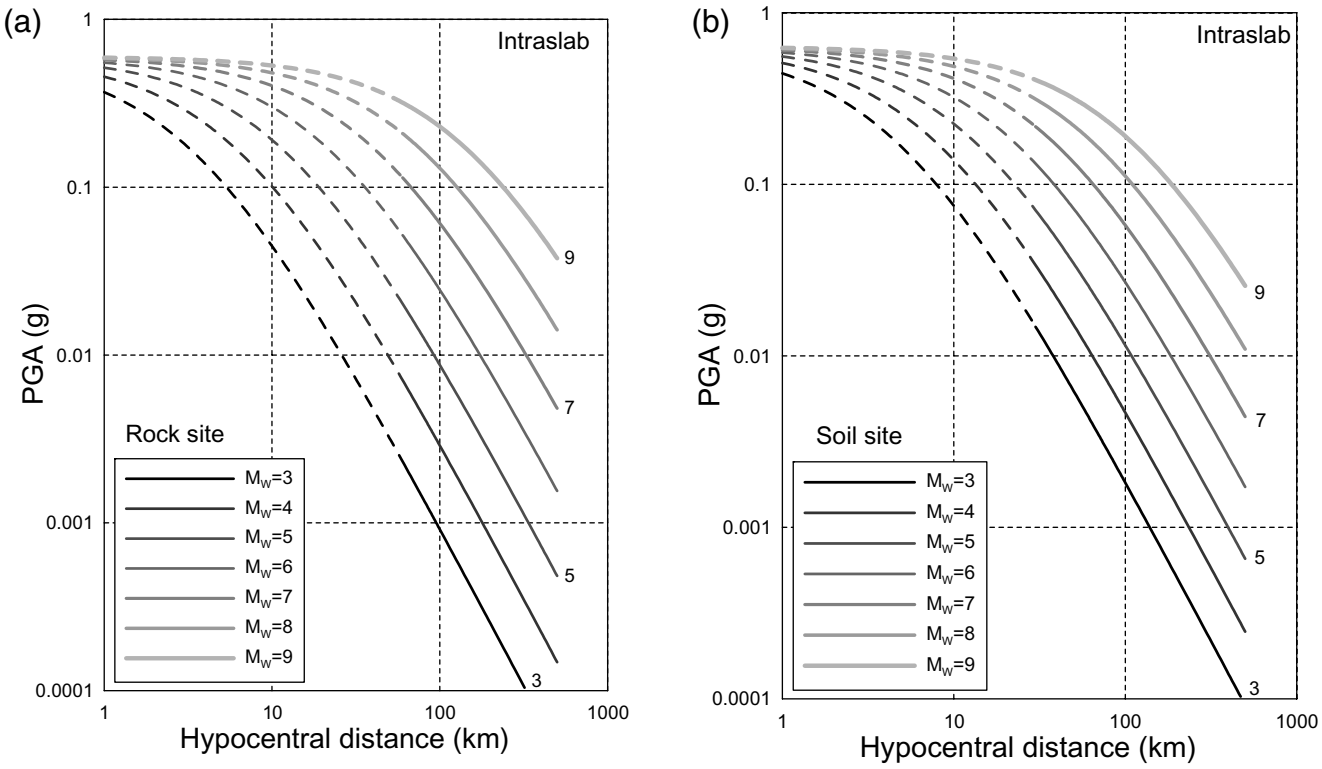

Figure 5. Results of the PGA attenuation curves for intraslab earthquakes at different magnitudes: (a) rock sites and (b) soil sites.

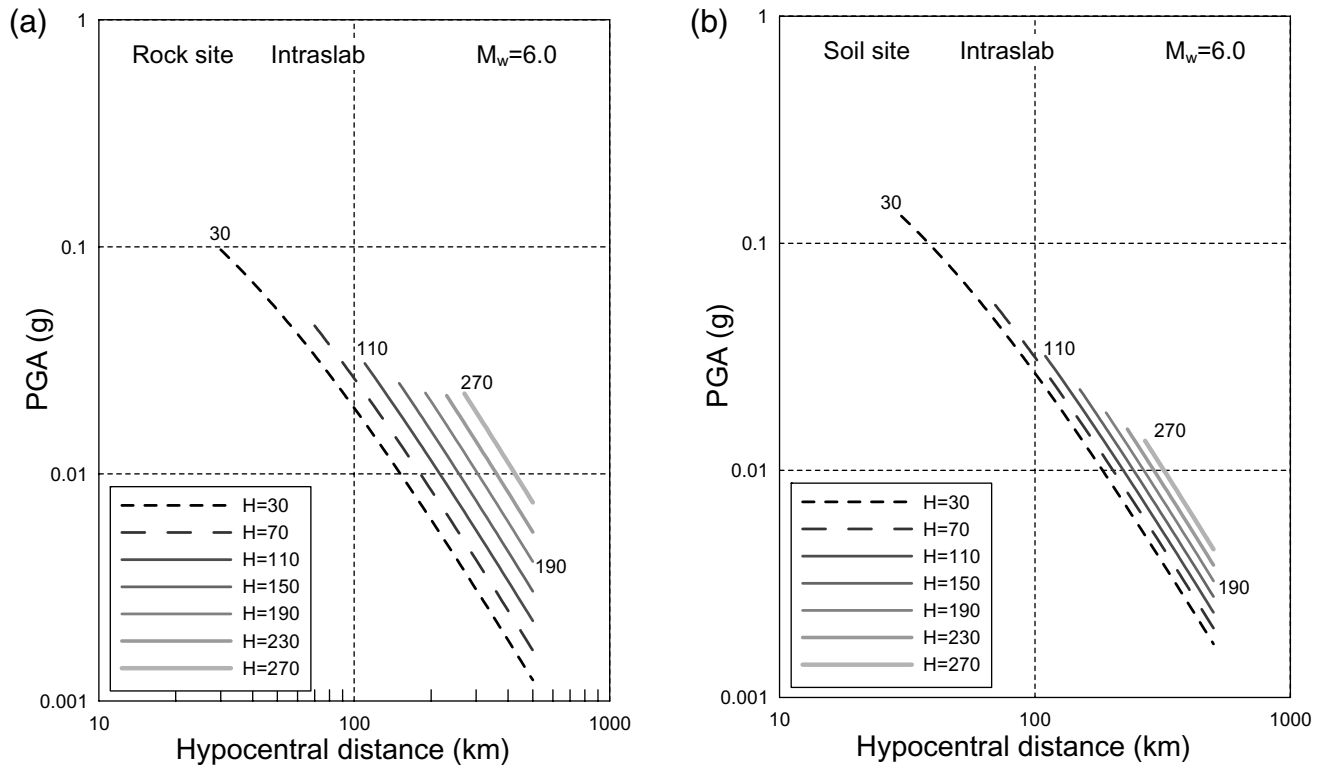

Figure 6. Results of the PGA attenuation curves for intraslab earthquakes at different depths: (a) rock sites and (b) soil sites.

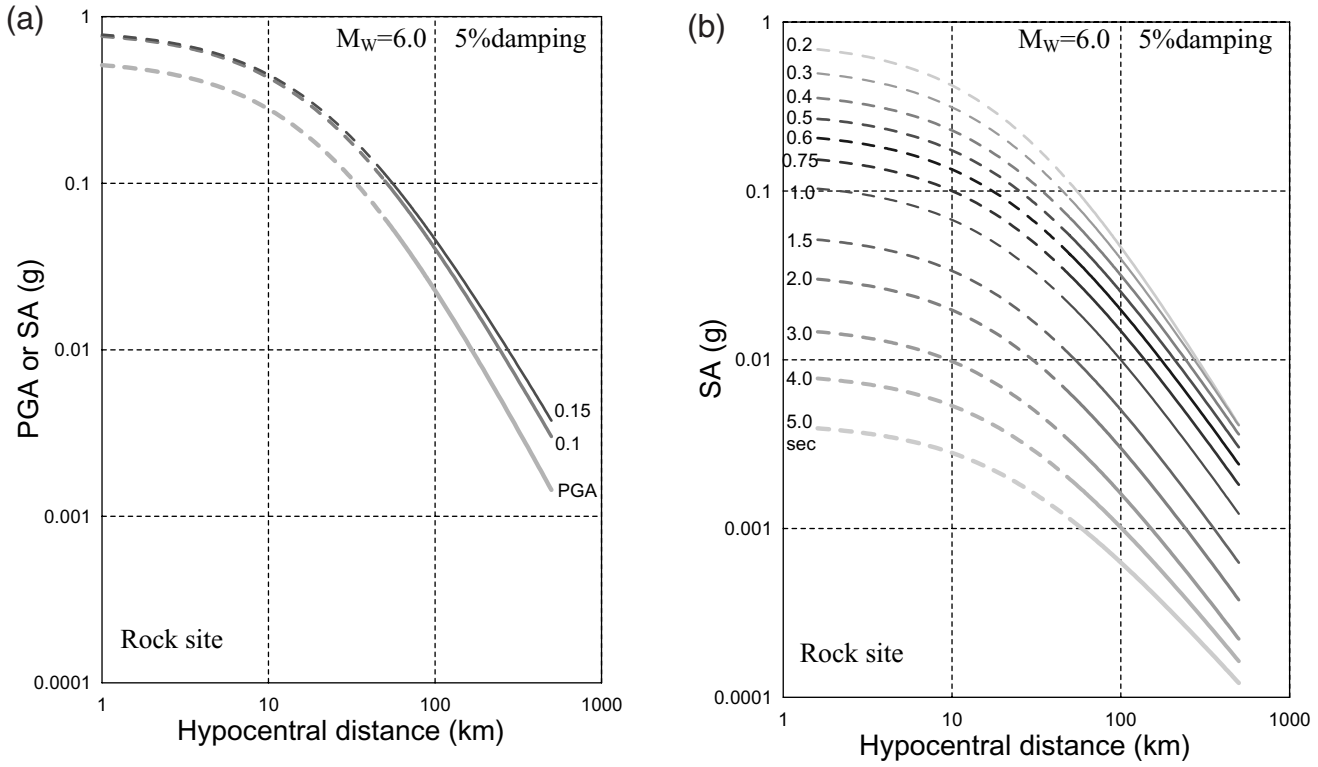

Figure 7. Results of the PGA and SA attenuation curves for intraslab earthquake, rock site, for periods from 0.1 to 5 sec; the magnitude is set to 6.0, and the damping is 5%.

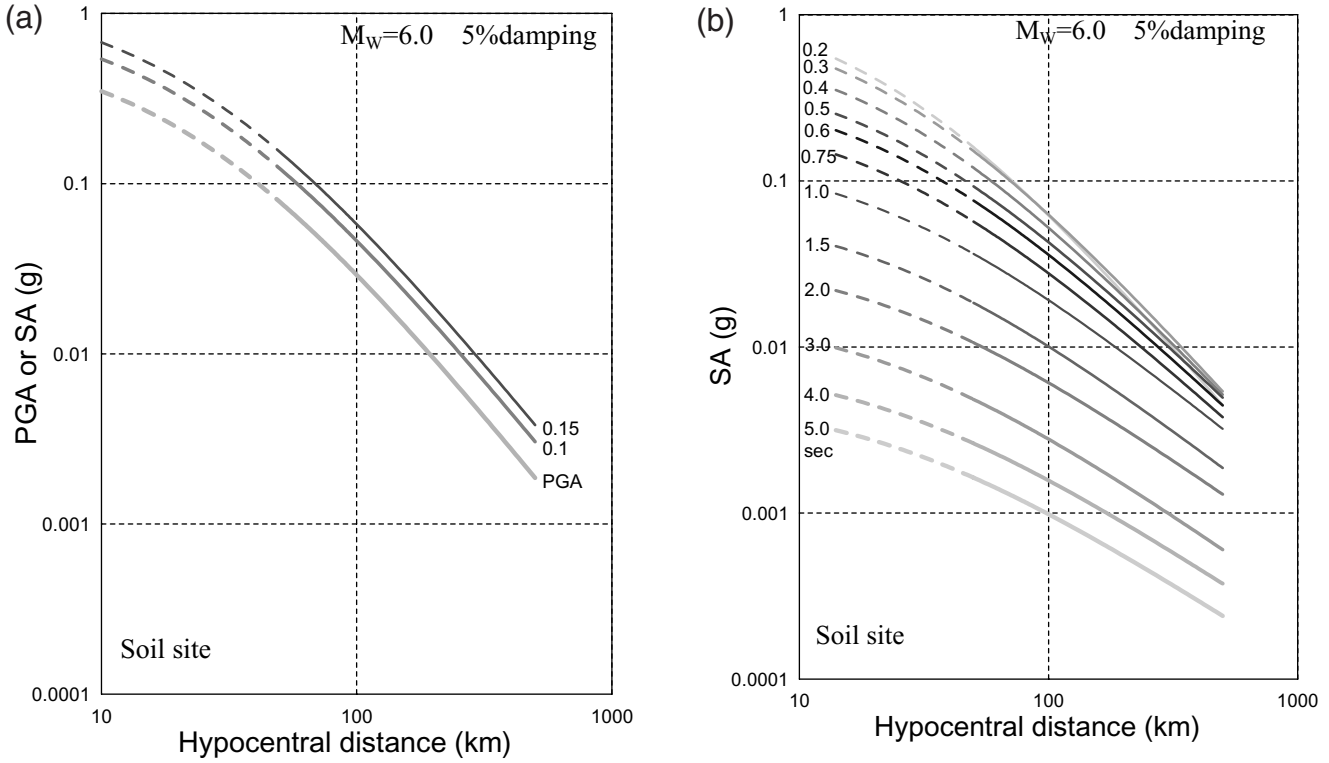

Figure 8. Results of the PGA and SA attenuation curves for intraslab earthquake, soil site, for periods from 0.1 to 5 sec; the magnitude is set to 6.0, and the damping is 5%.

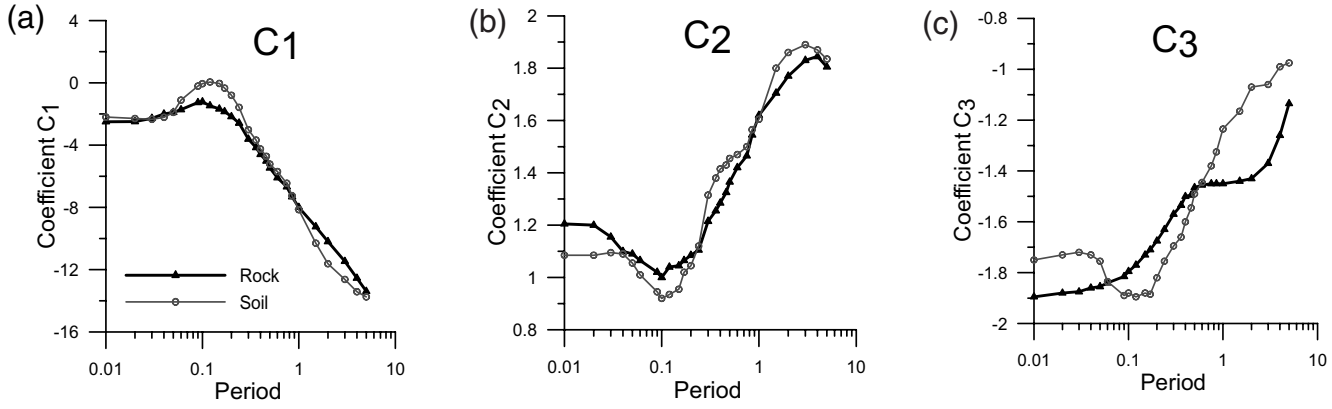

Figure 9. The variation of coefficients in the SA attenuation equations with the period 0.01–5.0 sec as listed in Tables 3 and 4; (a) coefficient C_1, (b) coefficient C_2, and (c) coefficient C_3.

error is assumed to have a lognormal distribution, that is, $\ln \varepsilon$ has a normal distribution. From the plot of the various regression errors $\sigma_{\ln \varepsilon}$ forms the SA attenuation equations for the various periods, it can be seen that the regression error increases as the period increases and then decreases after the long periods are reached (Fig. 10).

To confirm the results, we compared our new attenuation equations with the strong-motion data, separated into rock sites and soil sites for intraslab and interface earthquakes, as shown in Figures 11 and 12. These two events were selected because they are the events that contain the most recordings of intraslab and interface earthquakes. Most recorded data are distributed within the range between plus and minus one standard deviation of the mean attenuation curve. We also plotted a histogram of the residual and applied the optimal normal distribution curve that best fits the data, as shown in Figure 13. It can be seen that the residual fits a normal distribution very well, and the random error ε fits the lognormal distribution assumption.

Discussion

For the two types of subduction zone earthquakes, interface and intraslab, our results show a similar trend to those of Youngs *et al.* (1997) in terms of the difference between subduction zone earthquakes and crustal earthquakes, but there are some differences in the level of the predicted median values (Fig. 14). We found also the ground-motion level was higher for intraslab earthquakes than for interface earthquakes, by 20%–30%. This is consistent with the results

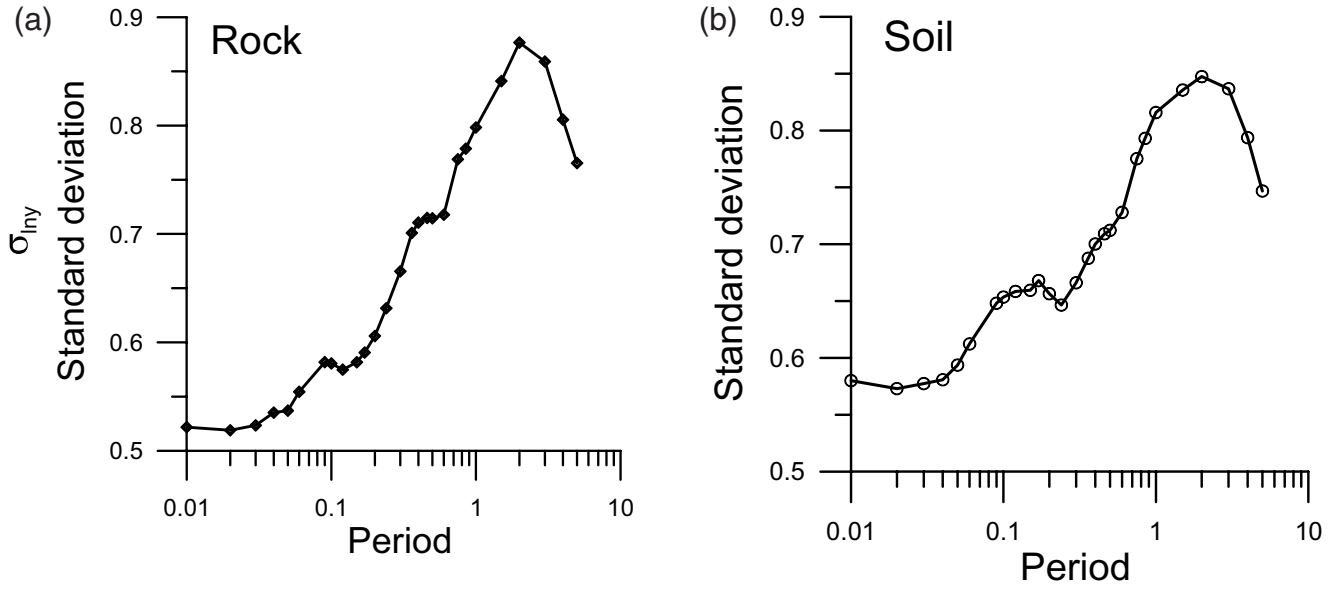

Figure 10. Variations of the standard deviation $\sigma_{\ln y}$ in the SA equations with the period 0.01–5.0 sec as listed in Tables 3 and 4: (a) rock sites and (b) soil sites.

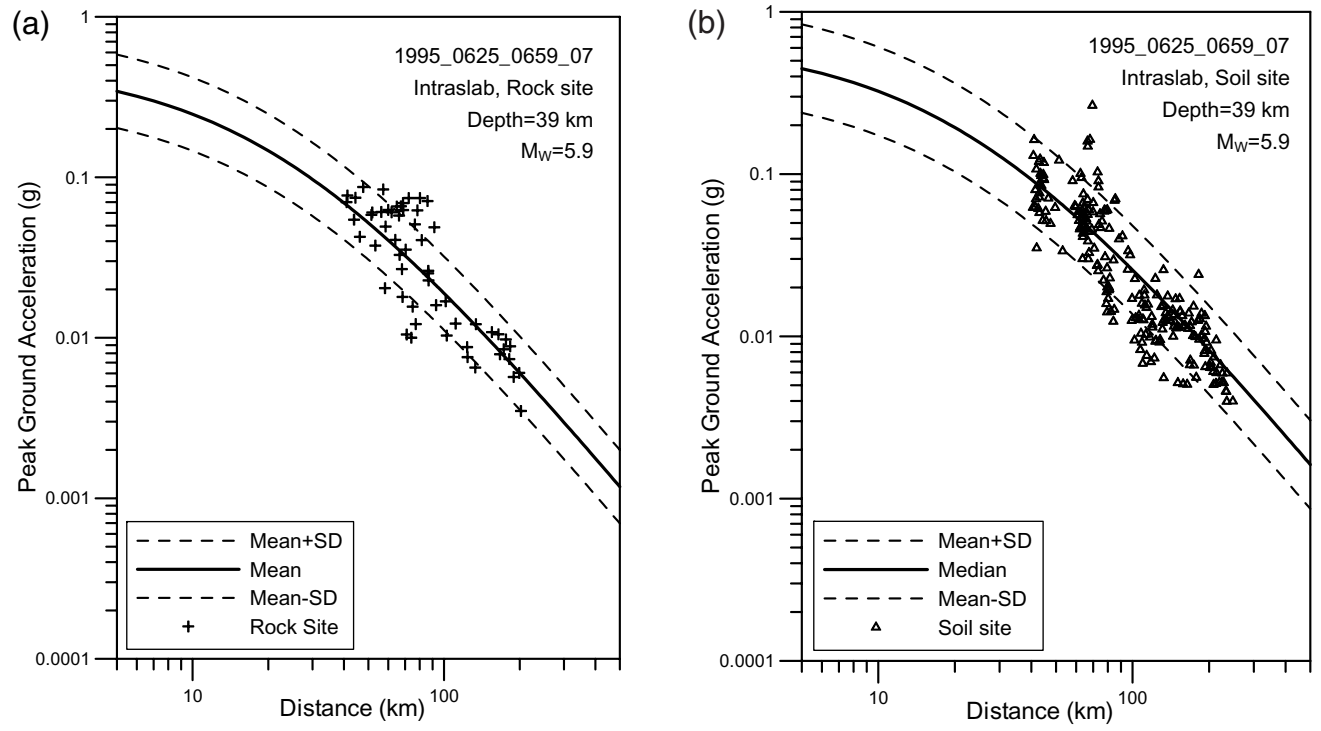

Figure 11. Comparison of the PGA data for M_w 5.9 intraslab earthquakes with the corresponding median and median $\pm\sigma$ attenuation equations listed in Table 3: (a) rock sites and (b) soil sites.

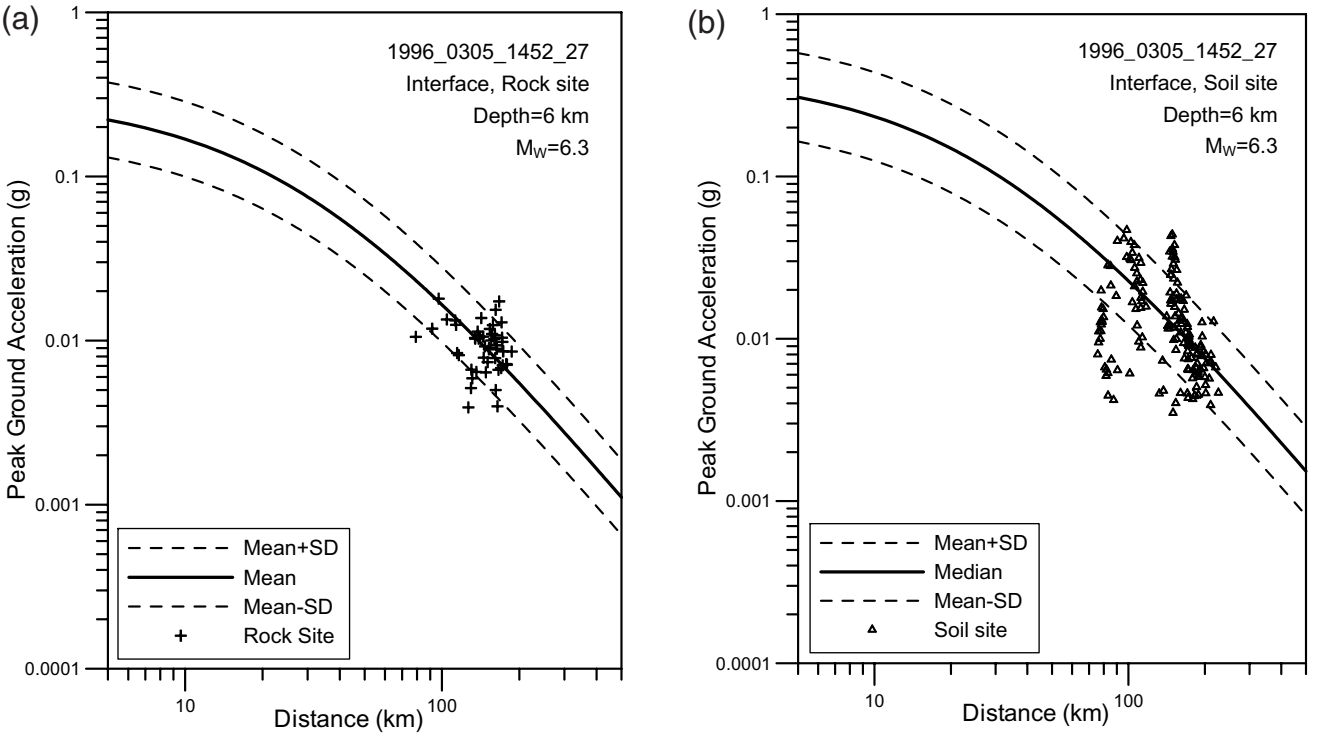

Figure 12. Comparison of the PGA data for M_w 6.3 interface earthquakes with the corresponding median and median $\pm\sigma$ attenuation equations listed in Table 3: (a) rock sites and (b) soil sites.

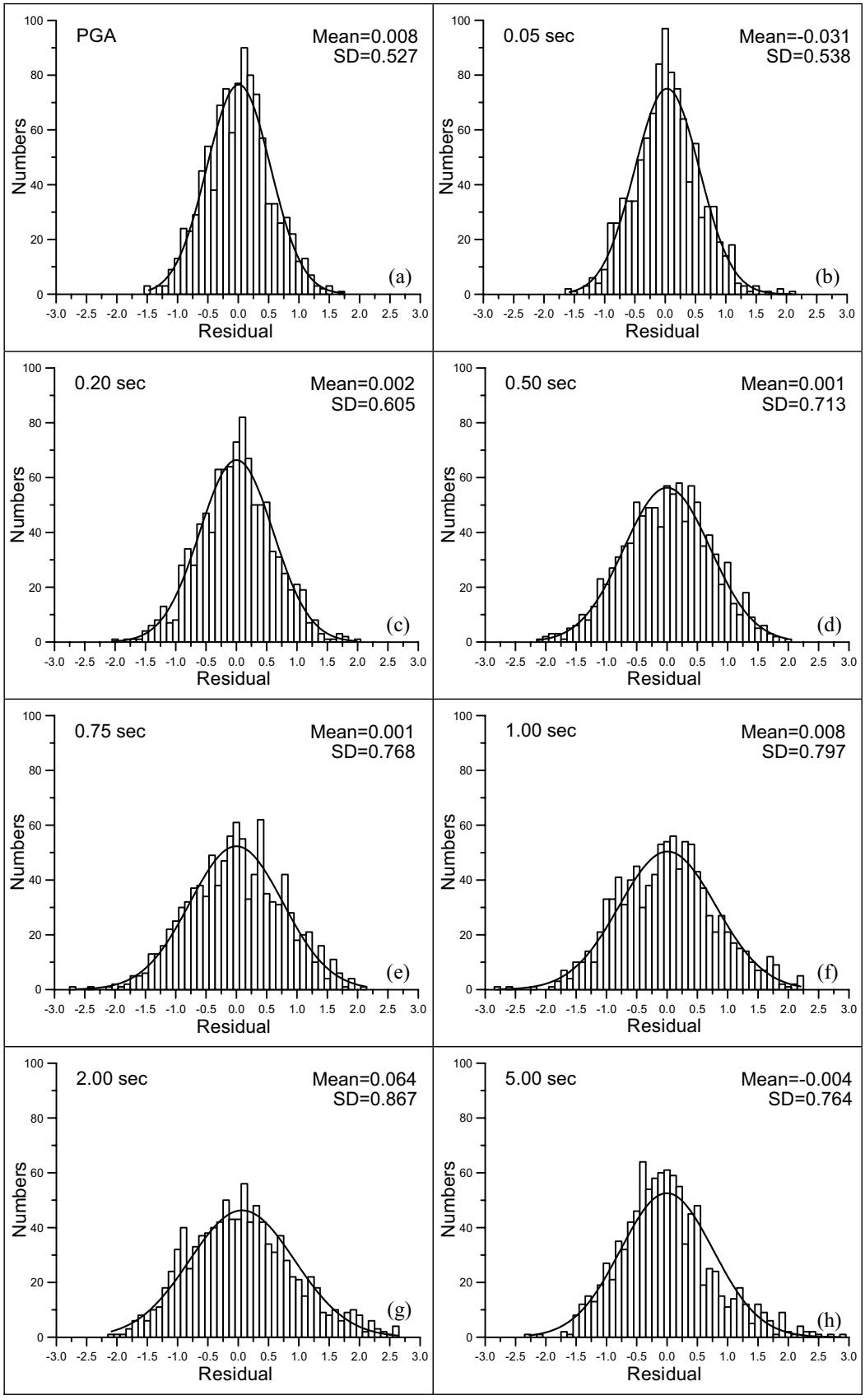

Figure 13. Histograms of $\ln y$ residual fitted to a normal distribution curve. Examples from SA equations for rock sites: (a) PGA, (b) 0.01 sec, (c) 0.02 sec, (d) 0.03 sec, (e) 0.04 sec, (f) 0.05 sec, (g) 0.06 sec, and (h) 0.09 sec.

obtained by Youngs *et al.* (1997) and Atkinson and Boore (2003), but the attenuation for intraslab earthquakes showed much stronger decay than for the interface earthquakes obtained by Atkinson and Boore.

Figure 14a reveals that higher ground-motion values would be predicted by the present attenuation equation than by the attenuation equations previously used in Taiwan (in Fig. 14a, Liu2005 represents Liu and Tsai [2005], Wu2001 represents Wu *et al.* [2001], and Chang 2001 crustal represents Chang *et al.* [2001]). Our results give the highest ground motion, except for the crustal attenuation developed by Chang *et al.* (2001) where there was apparently higher ground motion at distances greater than 100 km. Wu *et al.* (2001) and Liu and Tsai (2005) also used attenuation equations for crustal earthquakes but did not differentiate site classes. This is important for PSHA in Taiwan in that, at present, the ground-motion equations used by many other researchers lead to underestimation of the seismic hazard.

As can be seen in Figure 14b, our predicted ground-motion values are smaller than the values predicted by Youngs *et al.* (1997) (Youngs_ROCK and Youngs_SOIL in Fig. 14b) but are higher than the results of Atkinson and Boore (2003) (AB_ROCK and AB_SOIL in Fig. 14b). Atkinson and Boore (2003) predict a significant low value at *M* 6.0, as compared with others; however, the difference becomes smaller for larger magnitudes. Chang *et al.* (2001) predicted the highest ground-motion value (Chang 2001 subduction in Fig. 14b), but they did not divide the subduction zone earthquake category into interface and intraslab types, nor did they consider site classification.

This study reveals that, at a hypocentral distance of 50 km, the two types of sites for subduction zone earthquakes show changes in the normalized horizontal acceleration response spectrum (Fig. 15). The changes are in the following manner: (1) at periods greater than 0.3 sec and in rock sites the spectral acceleration increases with increasing magnitude, (2) changes in soil site SA are comparable to those for rock sites, except that the variance is greater, and (3) the maximum normalized SA tends to increase with increasing magnitude.

The relation between the normalized response spectrum and hypocentral distance for a subduction zone earthquake with a moment magnitude of 6.0 is shown in Figure 16. The normalized horizontal acceleration response spectrum for the two types of sites changes with the hypocentral distance. When the period of the SA of a rock site is greater than 0.1 sec, the normalized acceleration response spectrum increases with the hypocentral distance. When the period of the SA at the soil site exceeds 0.2 sec, the normalized response spectrum increases with the hypocentral distance; this increase is more distinct than for rock sites (Fig. 16).

We also compared the response spectra for the two types of sites to that of Youngs *et al.* (1997) and Atkinson and Boore (2003); see Figures 17 and 18. For *M* 7 and 8, our results are similar to that of these two papers for periods longer than 0.3 sec; our results show smaller values in short

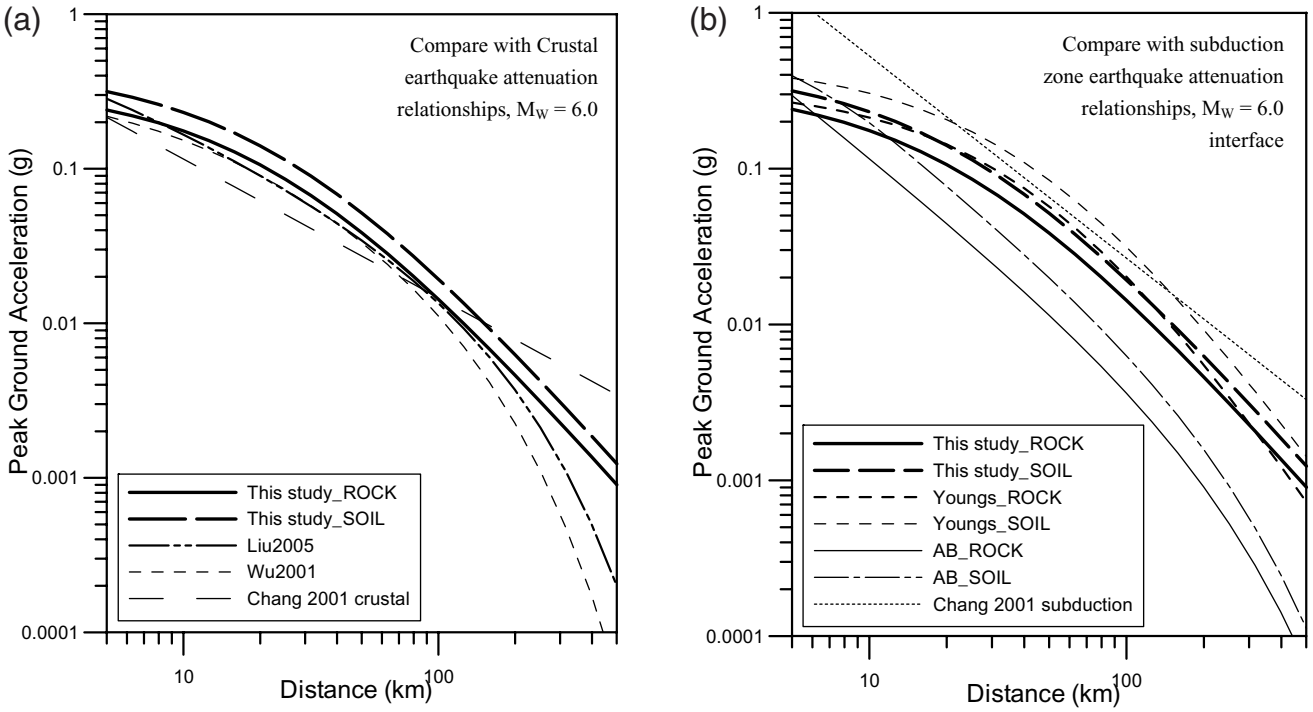

Figure 14. Comparison of the attenuation curves from results of this study and some other studies: (a) crustal earthquake attenuation equations published in Taiwan and (b) subduction zone earthquake attenuation equations.

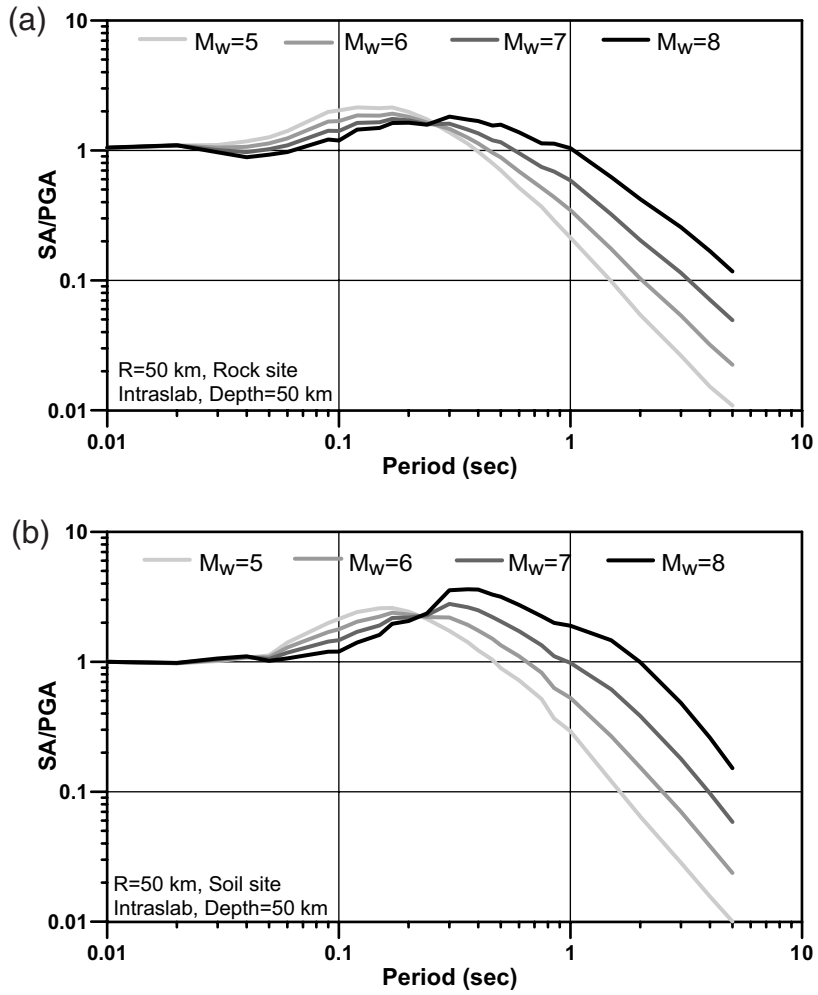

Figure 15. Variations of the spectral shapes with varying earthquake magnitude and fixed source-to-site distance at 50 km: (a) rock sites and (b) soil sites.

periods. For M 5 and 6, our results show smaller values than that of Youngs *et al.* (1997) for most periods but is larger for periods longer than 1 sec for soil sites. The latter may be due to the fact that we have used data from the Taipei Basin where deep soft soil and basin effect have been involved. The response spectrum predicted by Atkinson and Boore (2003) for M 5 and 6 was much smaller than ours. This may be because we used many data ranging from M 4 to 6, whereas a magnitude less than 5.5 is totally lacking in the data set of Atkinson and Boore (2003).

The definition of the earthquake magnitude parameter plays an important role in ground-motion attenuation analysis. The relevant M_L and M_w magnitude conversion equation previously developed in Taiwan was derived from shallow crustal earthquakes. If we used a shallow earthquake M_L–M_w relation to convert M_L of a deep earthquake to M_w, the same M_L will have larger M_w. But based on results shown in Figure 2b, for an M_L 6 earthquake it will have M_w 5.7 if a shallow earthquake M_L–M_w relation was used or M_w 5.5 if a deep earthquake M_L–M_w relation was used. The means for some subduction zone earthquakes did not have an M_w; if we use the M_L–M_w relation for shallow earthquakes as the conversion, the same ground-motion value will come from larger M_w. It is therefore necessary to formulate different a conversion equation for shallow earthquakes and deep earthquakes.

It has recently been discovered that there is a relationship between the attenuation equation and the focal depth (Crouse, 1991; Youngs *et al.*, 1997; Atkinson and Boore, 2003). This relationship has also been pointed out by Chang *et al.* (2001); however, their conclusions are not quite consistent. Chang *et al.* (2001) utilized data from 19 subduction zone earthquakes in the Taiwan area and found the depth index to be negative. This means that the ground-motion value decreases with increasing depth. This is different from the results for subduction zone earthquakes obtained by Youngs *et al.* (1997) and Atkinson and Boore (2003), as well as our result.

The decrease of earthquake ground-motion attenuation with increasing depth may be due to a path effect. In a sub-

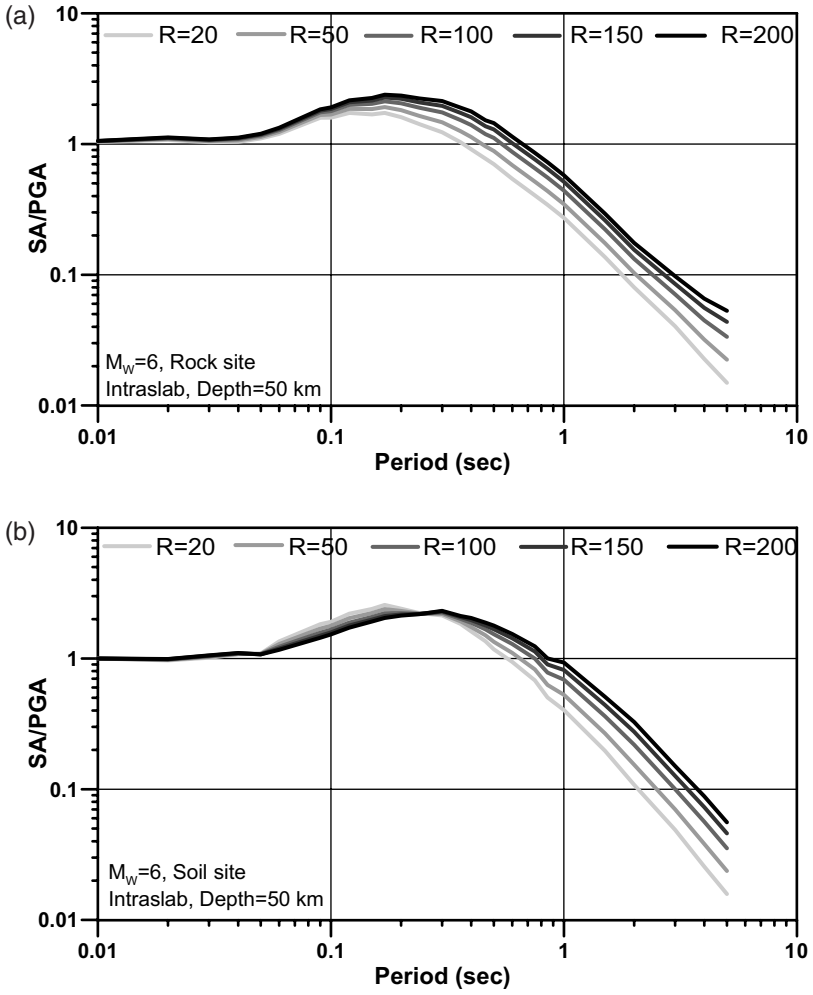

Figure 16. Variations of the spectral shapes with varying source-to-site distance and fixed earthquake magnitude at M_w 6.0: (a) rock sites and (b) soil sites.

duction system, the plate relative to the surrounding mantle will have a higher Q and slower attenuation. In other words, a seismic wave propagating within the interior of the plate will travel faster with less attenuation (Utsu, 1967; Utsu and Okada, 1968). With increasing depth, wave propagation will encounter a longer path with higher Q-values, leading to smaller attenuation, showing up in the attenuation equation as a depth effect.

Research on attenuation models has indicated that regression errors may change with differences in earthquake magnitude (Youngs *et al.*, 1995). We also conducted a similar analysis and got similar results. However, the number of large magnitude earthquakes in the Taiwan data set is quite limited; the variance for a small sample may not represent the variance of the entire population.

It is obvious that data has a profound effect on the analysis results. The northeastern Taiwan subduction zone earthquakes data lack large magnitude and far-field data. Thus, to use only these data to perform an analysis may result in a set of data bearing mathematical meaning but void of physical meanings for hazard analysis. This is why we added some larger magnitude subduction zone earthquakes from the world data set. However, a further study should be done to validate the suitability of adding these data.

Precision in regard to the location of an earthquake has a direct affect in the calculation of the distance and depth factors with the attenuation equation. In this study, relocation data was totally lacking. This precludes a discussion of the effects of earthquake location. However, the fact that most of earthquake data used in this study were located offshore of northeastern Taiwan means that the hypocentral distances were large so the effect of precise earthquake location should be negligible.

Conclusions and Recommendations

This study confirms that subduction zone earthquakes have lower attenuation than crustal earthquakes and that the ground-motion values predicted by these attenuation equations are higher than those obtained with the crustal

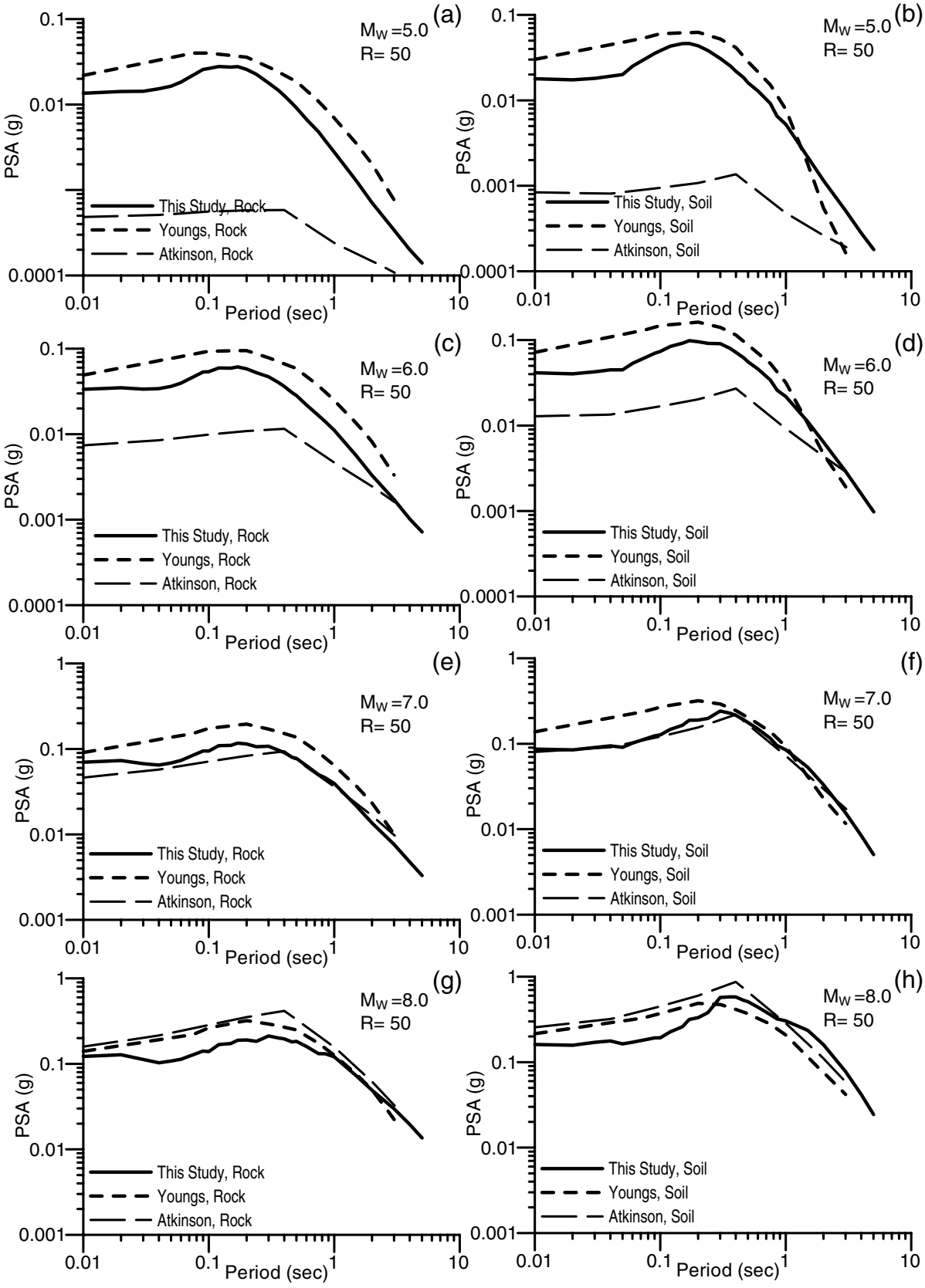

Figure 17. Comparison of the spectral shapes between the results of this study and those of Youngs *et al.* (1997) and Atkinson and Boore (2003) for different earthquake magnitudes with the source-to-site distance fixed at 50 km: (a), (c), and (e) rock sites and (b), (d), and (f) soil sites.

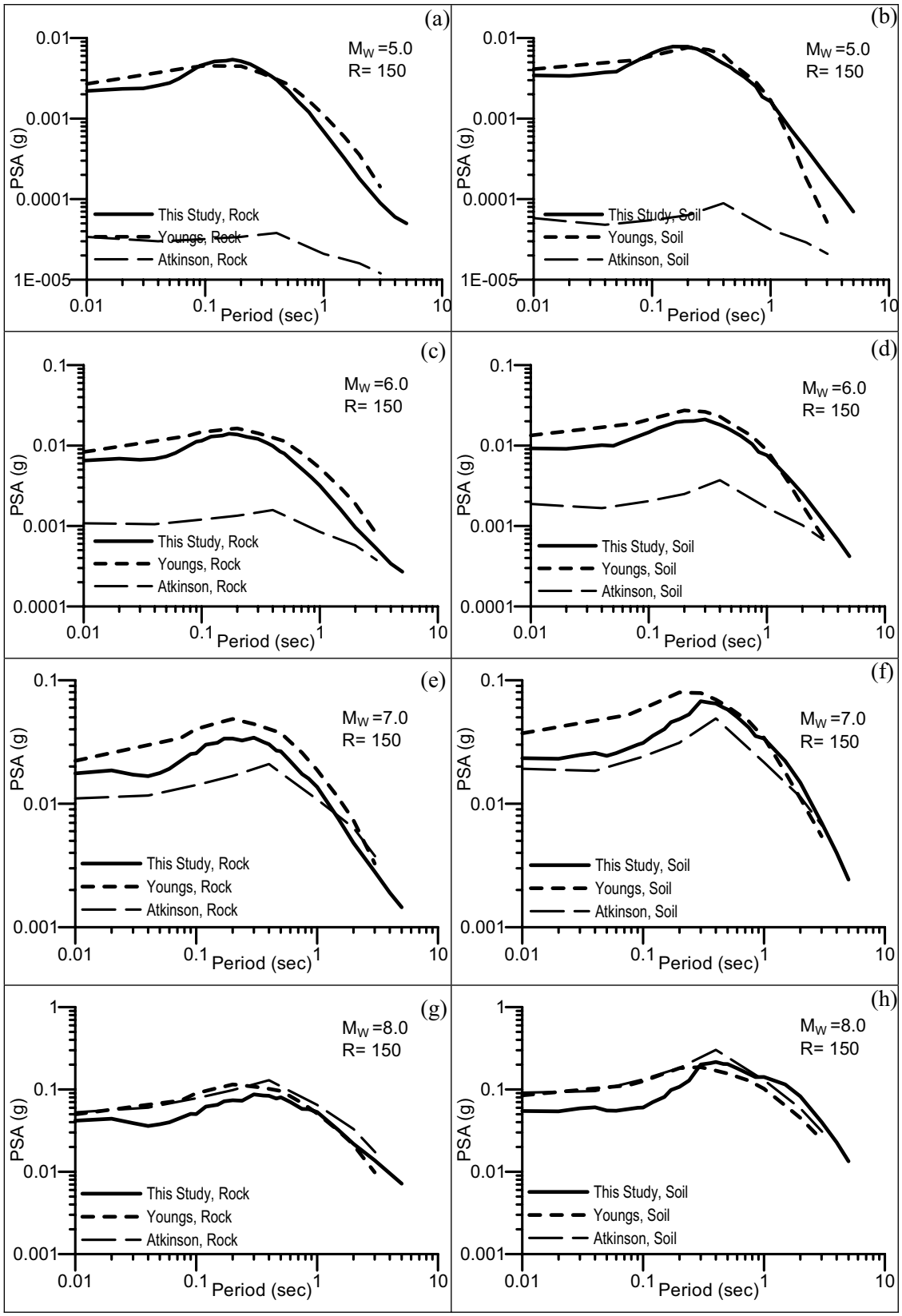

Figure 18. Comparison of the spectral shapes between the results of this study and those of Youngs *et al.* (1997) and Atkinson and Boore (2003) for different earthquake magnitudes with the source-to-site distance fixed at 150 km: (a), (c), and (e) rock sites and (b), (d), and (f) soil sites.

earthquake attenuation equations previously used. This has important implications for PSHA in Taiwan, because the present ground-motion equations used by many other researchers lead to an underestimation of the seismic hazard. The new attenuation equations should be applied. The PGA as well as SA attenuation equations and error analysis for various periods, for both rock sites and soil sites and for subduction zone interface and intraslab earthquakes in northeastern Taiwan, have been provided. The results may be used in the PSHA to establish a uniform hazard response spectrum for earthquake-resistant design and for safety evaluation of existing structures in Taiwan.

Compared with the subduction zone earthquake attenuation results obtained using worldwide data by Youngs *et al.* (1997), the estimated ground-motion level obtained in this study is lower for all magnitudes and all periods. This may reflect the characteristics of the northeastern Taiwan subduction zone and the local seismic-wave path.

The use of large magnitude foreign earthquake data is a temporary expedient. As more data from northeastern Taiwan become available, we need to redo this analysis. Also, instead of a least-square method, it is necessary to use a maximum likelihood method to resolve the problem of data distribution and the mixed effect model to treat the variance reasonably.

Acknowledgments

We extend our sincere thanks to the Seismology Center of the Central Weather Bureau, Taiwan, and to the Institute of Earth Sciences, Academia Sinica, Taiwan, for providing the strong-motion data. We also thank Yi-Ben Tsai and Hung-Chie Chiu for their valuable suggestions and reading of the manuscript. We would like to acknowledge Associate Editor Hiroshi Kawase and two anonymous reviewers for their valuable suggestions and comments that improved this article. This research was supported by the Taiwan Earthquake Research Center (TEC) funded through the National Science Council (NSC) with Grant Number NSC 96-2119-M-008-004. The TEC contribution number for this article is 00016.

References

Abrahamson, N. A., and K. M. Shedlock (1997). Overview, *Seism. Res. Lett.* **68,** 9–23.

Abrahamson, N. A., and W. J. Silva (1997). Empirical response spectral attenuation relations for shallow crustal earthquakes, *Seism. Res. Lett.* **68,** 94–127.

Atkinson, G. M., and D. M. Boore (2003). Empirical ground-motion relations for subduction-zone earthquakes and their application to Cascadia and other regions, *Bull. Seismol. Soc. Am.* **93,** 1703–1729.

Campbell, K. W. (1981). Near-source attenuation of peak horizontal acceleration, *Bull. Seismol. Soc. Am.* **71,** 2039–2070.

Campbell, K. W. (1997). Empirical near-source attenuation relationships for horizontal and vertical components of peak ground acceleration, peak ground velocity, and pseudo-absolute acceleration response spectra, *Seism. Res. Lett.* **68,** 154–179.

Chang, T. Y., F. Cotton, and J. Angelier (2001). Seismic attenuation and peak ground acceleration in Taiwan, *Bull. Seismol. Soc. Am.* **91,** 1229–1246.

Chen, T. H. (1991). The study on the attenuation of maximum peak ground motion in Taiwan, *Master's Thesis*, National Central University, Taiwan (in Chinese).

Chen, Y. L. (1995). Three dimensional velocity structure and kinematic analysis in Taiwan area, *Master's Thesis*, National Central University, Taiwan, 172 p (in Chinese).

Cheng, S. N., and Y. T. Yeh (1989). Catalog of the earthquakes in Taiwan from 1604 to 1988, Institute of Earth Sciences Report IES-R-661, Academia Sinica, Taiwan, 255 pp (in Chinese).

Crouse, C. B. (1991). Ground-motion attenuation equation for earthquake on Cascadia subduction-zone earthquake, *Earthq. Spectra* **7,** 210–236.

Crouse, C. B., K. V. Yogesh, and B. A. Schell (1988). Ground motions form subduction zone earthquakes, *Bull. Seismol. Soc. Am.* **78,** 1–25.

Fukushima, Y., and T. Tanaka (1990). A new attenuation relation for peak horizontal acceleration of strong earthquake ground motion in Japan, *Bull. Seismol. Soc. Am.* **80,** 757–783.

Hanks, T. C., and H. Kanamori (1979). A moment magnitude scale, *J. Geophys. Res.* **84,** 2348–2350.

Heaton, T., F. Tajima, and A. W. Mori (1986). Estimating ground motions using recorded accelerograms, *Surv. Geophys.* **8,** 25–83.

Hong, L. L., and M. D. Hsu (1993). Seismic hazard analysis base on random field simulation, report for Hazard Mitigation Technology Research 82-12, National Science Council, 91 pp (in Chinese).

Hsu, M. T. (1983). Estimation of earthquake magnitudes and seismic intensities of destructive earthquakes in the Ming and Ching eras, *Meteorol. Bull.* **29,** no. 4, 1–18 (in Chinese with English abstract).

Huang, G. C., H. Kao, and Y. M. Wu (2000). The relationship between M_L and M_W for regional earthquakes in Taiwan, *Proceedings of the Annual Meeting of the Chinese Geophysical Society*, Taipei, Taiwan, 193–201.

Hwang, J. Y. (1995). Characteristics of strong ground and analysis of seismic hazard in Taiwan area, *Master's Thesis*, National Central University, Taiwan, 110 pp (in Chinese).

Joyner, W. B., and D. M. Boore (1981). Peak horizontal acceleration and velocity from strong-motion records including records from the 1979 Imperial Valley, California, earthquake, *Bull. Seismol. Soc. Am.* **71,** 2011–2038.

Kanai, K., K. Hisrano, S. Yoshizawa, and T. Asada (1966). Observation of strong earthquake motion in Matsushiro area, part 1, *Bull. Earthq. Res. Inst., Univ. of Tokyo* **44,** 1269–1296 (In Japanese).

Kao, H., S. J. Shen, and K.-F. Ma (1998). Transition from oblique subduction to collision: earthquakes in the southernmost Ryukyu arc-Taiwan region, *J. Geophys. Res.* **103,** 7211–7229.

Lee, C. T., C. T. Cheng, C. W. Liao, and Y. B. Tsai (2001). Site classification of Taiwan free-field strong-motion stations, *Bull. Seismol. Soc. Am.* **91,** 1283–1297.

Liu, K. S. (1999). Attenuation relations for strong seismic ground motion in Taiwan, *Ph.D. Thesis*, National Central University, Taiwan, 240 pp (in Chinese with English abstract).

Liu, K. S., and Y. B. Tsai (2005). Attenuation relationships of peak ground acceleration and velocity for crustal earthquake in Taiwan, *Bull. Seismol. Soc. Am.* **95,** 1045–1058.

Liu, K. S., T. C. Shin, and Y. B. Tsai (1999). A free field strong motion network in Taiwan: TSMIP, *TAO* **10,** 377–396.

Loh, J. S. (1996). The parameters about the strong motion characteristics and the evaluation of seismic hazards, Criterions of Evaluating and Enhancing the Security from the Shockproof in the System of Telecommunication and Transportation, Ministry of Transportation and Communications, R.O.C., 2–3 (in Chinese).

Molas, G. L., and F. Yamazaki (1995). Attenuation of earthquake ground motion in Japan including deep focus event, *Bull. Seismol. Soc. Am.* **85,** 1343–1358.

Ni, S. T., and H. J. Chiu (1991). Discussion on the attenuation statistical models from maximal strong motion data of Taiwan, in *Proceedings of the 3rd Taiwan Symposium on Geophysics*, Taipei, Taiwan, October, 95–105 (in Chinese).

Rau, R. J., and F. T. Wu (1995). Tomographic imaging of lithospheric structures under Taiwan, *Earth Planet. Sci. Lett.* **133,** 517–532.

Richter, C. F. (1958). *Elementary Seismology*, W. H. Freeman, San Francisco, California.

Russell, S. J., and P. Norvig (2003). *Artificial Intelligence: A Modern Approach*, Second Ed., Prentice Hall, New York, 111–114.

Sadigh, K., C. Y. Chang, J. A. Egan, F. Makdisi, and R. R. Youngs (1997). Attenuation relationships for shallow crustal earthquakes based on California strong motion data, *Seism. Res. Lett.* **68,** 180–189.

Seno, T. (1977). The instantaneous rotation vector of the Philippine Sea plate relative to Eurasian plate, *Tectonophysics* **42,** 209–226.

Seno, T., S. Stein, and A. E. Gripp (1993). A model for the motion of the Philippine Sea Plate consistent with NUVEL-1 and geological data, *J. Geophys. Res.* **98,** 941–948.

Shen, S. S. (1996). Characteristics of subduction and collision structures in northeastern Taiwan from earthquake mechanisms determined by body waveform inversion, *Master's Thesis*, National Central University, Taiwan, 177 pp (in Chinese).

Shin, T. C. (1998). A preliminary study of earthquake early warning system in the Taiwan area, *Meteorol. Bull.* **42,** no. 2, 118–134 (in Chinese with English abstract).

Tichelaar, B. W., and L. J. Ruff (1993). Depth of seismic coupling along subduction zones, *J. Geophys. Res.* **98,** 2017–2037.

Toro, G. R., N. A. Abrahamson, and J. F. Schneider (1997). Model of strong ground motions from earthquakes in central and eastern North America: best estimates and uncertainties, *Seism. Res. Lett.* **68,** 41–57.

Tsai, C. C. P. (1998). Ground motion modeling in the near-source regime: a barrier model, *TAO* **9,** 15–30.

Tsai, Y. B., and B. A. Bolt (1983). An analysis of horizontal peak ground acceleration and velocity from SMART 1 array data, *Bull. Inst. Earth Sci.* **3,** 105–126.

Tsai, Y. B., and K. L. Wen (1999). NAPHM 87-07, Compilation of a uniform catalog of earthquakes in Taiwan and development of motion attenuation relationships, report of the National Science and Technology Program for Hazards Mitigation, 79 pp.

Tsai, C. C., C. H. Loh, and Y. T. Yeh (1987). Analysis of earthquake risk in Taiwan based on seismotectonic zones, *Mem. Geol. Soc. China* **9,** 413–446.

Utsu, T. (1967). Anomalies in seismic wave velocity and attenuation associated with a deep earthquake zone (1), *J. Fac. Sci., Hokkaido Univ. Ser. 7 Geophys.* **3,** 1–25.

Utsu, T., and H. Okada (1968). Anomalies in seismic wave velocity and attenuation associated with a deep earthquake zone (2), *J. Fac. Sci., Hokkaido Univ. Ser. 7 Geophys.* **3,** 65–84.

Wang, T.-T. (1991). The characteristics of the acceleration response spectra for the Lo-Tung area, *Master's Thesis*, National Central University, Taiwan (in Chinese).

Wu, Y. M., T. C. Shin, and C. H. Chang (2001). Near real-time mapping of peak ground acceleration and peak ground velocity following a strong earthquake, *Bull. Seismol. Soc. Am.* **91,** 1218–1228.

Youngs, R. R., N. A. Abrahamson, F. Makdisi, and K. Sadigh (1995). Magnitude dependent dispersion in peak ground acceleration, *Bull. Seismol. Soc. Am.* **85,** 1161–1176.

Youngs, R. R., S. J. Chiou, W. J. Silva, and J. R. Humphrey (1997). Strong ground motion attenuation relationships for subduction zone earthquakes, *Seism. Res. Lett.* **68,** 58–73.

Yu, S. B., H. Y. Chen, and L. C. Kuo (1997). Velocity field of GPS stations in the Taiwan area, *Tectonophysics* **274,** 41–59.

Institute of Geophysics
National Central University
No. 300, Jhongda Rd.
Chung-Li City, Taoyuan County, Taiwan 32001
person@gis.geo.ncu.edu.tw
(P.-S.L.)

Institute of Applied Geology
National Central University
No. 300, Jhongda Rd.
Chung-Li City, Taoyuan County, Taiwan 32001
ct@gis.geo.ncu.edu.tw
(C.-T.L.)

Manuscript received 6 January 2006